The Contribution of Salt Fingers to Vertical Mixing in the North Atlantic Tracer Release Experiment*

LOUIS ST. LAURENT

MIT/WHOI Joint Program, Woods Hole Oceanographic Institution, Woods Hole, Massachusetts

RAYMOND W. SCHMITT

Woods Hole Oceanographic Institution, Woods Hole, Massachusetts

ABSTRACT

The North Atlantic Tracer Release Experiment (NATRE) was performed in an area moderately favorable to salt fingers. However, the classic finger signature of a distinct thermohaline staircase caused by upgradient density flux was absent. This is likely because mixing by turbulence was sufficiently strong to disrupt the formation of permanent step and layer systems. Despite the lack of a staircase, optical shadowgraph profiles revealed that small-scale tilted laminae, previously observed in a salt-finger staircase, were abundant at the NATRE site. Using microstructure observations, the strength of salt-finger mixing has been diagnosed using a nondimensional parameter related to the ratio of the diffusivities for heat and buoyancy (Γ, ''the dissipation ratio''). By examining the dissipation ratio in a parameter space of density ratio (R_ρ) and Richardson number (Ri), the signal of salt fingers was discerned even under conditions where turbulent mixing also occurred. While the model for turbulence describes most dissipation occurring when Ri < 1, dissipation at larger Ri is better described by the salt-finger model. Based on the results of the parameter space analysis, a method is proposed for estimating the salt-finger enhancement of the diapycnal haline diffusivity (k_s) over the thermal diffusivity (k_θ). During April 1992 at the NATRE site, it was found that $k_\theta = (0.08 \pm 0.01)$ cm^2 s^{-1} and $k_s = (0.13 \pm 0.01)$ cm^2 s^{-1} for the neutral density surface local to the tracer release isopycnal ($\sigma_\theta \sim 26.75$ kg m^{-3}, $z \sim 300$ m). The flux divergence of buoyancy was also computed, giving the diapycnal advection $w_* = -(1.7 \pm 1.2)$ m yr^{-1}. Moreover, divergence of vertical buoyancy flux was dominated by the haline component. For comparison, the tracer release method gave a diffusivity of $k_s = (0.12 \pm 0.02)$ cm^2 s^{-1} (May–November 1992) and a diapycnal velocity of $w_* = -(3 \pm 1)$ m yr^{-1} (May 1992–November 1994) at this site. The above numbers are contrasted to diffusivity estimates derived from turbulence theory alone. Best agreement between tracer-inferred mixing rates and microstructure based estimates is achieved when the salt-finger enhancement of k_s is taken into account.

1. Introduction

Dissipation rates of thermal variance (χ) and turbulent kinetic energy (TKE, ϵ) are used to infer diapycnal fluxes of heat, salt, and density in the ocean. The divergence of the density flux will dictate the strength of the diapycnal advection. Further dynamics are set by the vertical divergence of the diapycnal advection, which provides the vorticity forcing in the ocean's interior. Thus, in a fundamental way, the general circulation of the ocean is influenced by the second derivatives of the dissipation rates with respect to the vertical. This work will examine the problem of estimating the diapycnal advection from observations of χ and ϵ in a region influenced by the salt-finger form of double-diffusive convection.

Many regions of the World Ocean are characterized by haline stratification that is top heavy with respect to density. Such regions include the Mediterranean outflow, the western tropical North Atlantic, and the ''central waters'' of the subtropical gyres (Schmitt 1994). The unstable potential energy stored in the top-heavy salinity stratification may be released in small-scale convection cells known as ''salt fingers.'' The vertical fluxes produced by the finger instability act to diffuse concentrations of heat and salt down their mean gradients. While convecting plumes (fingers) generally preserve their salinity variance, thermal variance is lost to the molecular conduction of heat across individual cell boundaries. Hence, fingers act to vertically transport salinity more efficiently than heat. The haline component of the buoyancy flux exceeds the thermal com-

Corresponding author address: Louis St. Laurent, MIT/WHOI Joint Program, MS #21, Woods Hole Oceanographic Institution, Woods Hole, MA 02543.
E-mail: lstlaurent@whoi.edu

ponent, resulting in an upgradient flux of density. Mixing by salt fingers may be modeled in terms of separate eddy diffusivities for heat (k_θ), salt (k_s), and density (k_ρ). While the finger fluxes of heat and salt are both down their respective gradients, with $k_s > k_\theta > 0$, the finger flux of density is upgradient so that $k_\rho < 0$. This upgradient flux of density has been shown to form and maintain a thermohaline staircase, in which a series of well-mixed layers are separated by sharp interfaces (Stern and Turner 1969). Such staircases have been observed at the Mediterranean outflow, the Tyrrhenian Sea, and in the tropical Atlantic near Barbados (Schmitt et al. 1987). The existence of a thermohaline staircase is taken to be a strong indicator of salt-finger mixing.

However, staircases are not always found in open-ocean regions having finger-favorable stratification. In general, the upgradient density flux induced by salt fingers will be opposed by downgradient turbulent fluxes produced by internal wave breaking. Unlike salt-finger mixing, the high Reynolds number turbulence occurring in the ocean produces fluxes of heat and salt that are uninfluenced by differences in molecular properties, resulting in uniform diffusivities among scalars (i.e., $k_\theta = k_s = k_\rho$). Thus, in a region experiencing both salt-finger and turbulent fluxes, the magnitude and direction of the net buoyancy flux is then determined by the competition between the two processes. To properly determine the buoyancy flux in these regimes, a means of assessing both the relative occurrence and magnitude of the two processes is needed. The need for a procedure allowing calculation of the net k_ρ in a region with both turbulence and salt fingers serves as the primary motivation for this study.

The work presented here will rely on observations of microscale dissipation obtained from the free falling high-resolution profiler (HRP; Schmitt et al. 1987), as a means of assessing the diapycnal fluxes occurring in the thermocline at the North Atlantic Tracer Release Experiment (NATRE) site. A previous comparison of microstructure-derived diffusivities (Toole et al. 1994) and tracer-derived diffusivities (Ledwell et al. 1993) has indicated general agreement. This paper will strive to identify the turbulent and salt-finger contributions to the net diffusivities. Furthermore, we will allow for the possible elevation of the haline diffusivity over the thermal diffusivity, as well as the possibility for a negative density diffusivity. We will establish a means of identifying both the relative frequency and magnitude of salt-finger and turbulent dissipation events utilizing several nondimensional parameters available from quantities measured by the HRP. The density ratio $R_\rho = (\alpha\Theta_z)(\beta S_z)^{-1}$ is the parameter that dictates a system's susceptibility to double-diffusive instability. The salt-finger instability is permitted if $1 < R_\rho < 100$ (Schmitt 1979a). However, in an ocean constantly perturbed by internal wave strain, modes of instability with characteristic period longer than that of the wave field ($2\pi N^{-1}$) may fail to grow. For this reason Schmitt and Evans (1978) suggest only

modes with growth rates near N will become strongly established, this being true if $1 < R_\rho < 2$. A second parameter, the gradient Richardson number Ri = $N^2 U_z^{-2}$, measures a system's susceptibility to shear (U_z) instability. While much work has focused on the Ri < 0.25 instability condition, Polzin (1996) found a general increase in turbulent dissipation when Ri < 1. Finally, we will use the nondimensional ratio of the dissipation rates $\Gamma = (\chi N^2)(2\epsilon\Theta_z^2)^{-1}$. This quantity, "the dissipation ratio," is related to both mixing efficiency (R_f) and the ratio of the diffusivities for heat and buoyancy. Models for this parameter have been formulated for both turbulence (Oakey 1985) and salt-finger mixing (Hamilton et al. 1989; McDougall and Ruddick 1992). Ruddick et al. (1997) have examined dissipation at the NATRE site in a similar manner, using R_ρ, Γ, and the nondimensional TKE dissipation parameter $\epsilon(\nu N^2)^{-1}$ (a Reynolds number). Ruddick et al. (1997) fail to find any significant signal of salt fingering. However, the gradient Richardson number provides a strong constraint for identifying turbulence produced by shear instability, and we will show that the parameter family of R_ρ, Ri, and Γ is sufficient for isolating the signal of salt fingers even in conditions where turbulence is also occurring.

We will begin by describing some qualitative evidence for salt fingers at the NATRE site (section 2). Quantitative evidence for salt-finger mixing in terms of dissipation data is presented in section 3. We give a description of HRP data (section 3a), present a model of the dissipation ratio (section 3b), discuss the method of analysis (section 3c), discuss the statistical treatment of dissipation data (section 3d), and present our results (section 3e). The results of the (R_ρ, Ri, Γ) parameter analysis are then applied to the NATRE profile data to estimate the net diffusivities of heat and salt (section 4a) and the diapycnal advection (section 4b). We present a discussion of this material in section 5.

2. Qualitative evidence for salt fingers at the NATRE site

The North Atlantic Tracer Release Experiment was conducted in the Canary Basin of the eastern North Atlantic. A 150-station microstructure survey of the release site was completed prior to the tracer release phase of the experiment, discussed by Ledwell et al. (1993, 1998). Measurements were made using a free falling, autonomously profiling instrument, the high-resolution profiler. The HRP produces measurements of temperature, conductivity, and velocity at both finescale [$O(1$ m)] and microscale [$O(1$ cm)] resolution. Measurements of optical microstructure were also made using a shadowgraph imaging system. Descriptions of the HRP and all of its component instruments, including the shadowgraph, are given by Schmitt et al. (1988).

The NATRE site rests within the central waters of the North Atlantic subtropical gyre (Fig. 1). Several studies (Schmitt and Evans 1978; Schmitt 1981; Schmitt 1990)
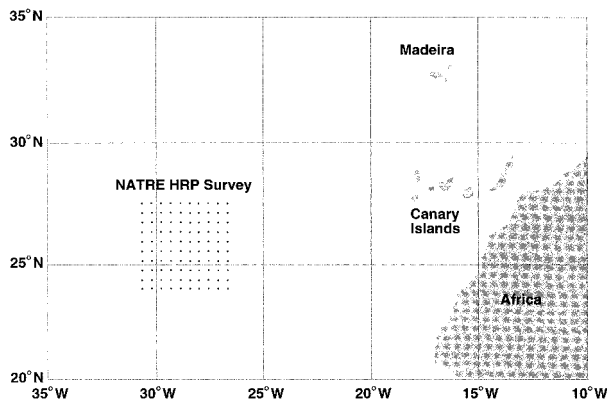
FIG. 1. Location of the NATRE HRP survey. Over 150 dives were completed over 26 days. The survey consisted of the 100 station grid spanning the $(400 \text{ km})^2$ region shown. An additional 50 stations were tightly centered about (26°N, −28°W). The HRP survey was completed two weeks prior to the tracer-release phase of the experiment.

FIG. 2. A section showing 10 profiles of the density ratio R_ρ, $= (\alpha \langle \Theta_z \rangle)(\beta \langle S_z \rangle)^{-1}$. The gradients were calculated using a 5-m scale, smoothed using a 50-m running average. Stations 3–12 constitute the meridional section at the western edge of the survey. Each successive station is offset two R_ρ units, and the reference value $R_\rho = 2.0$ is shown for each profile. There is large variability in the mixed layer and beneath $z = 600$ m due to intrusive features.

have argued that salt fingers contribute to the vertical mixing in this region. In particular, these studies argue that finger mixing should dominate turbulent mixing if $R_\rho \lesssim 2$. Indeed, this describes the density ratio structure in the upper 500 m of the NATRE site thermocline (Fig. 2). However, no permanent thermohaline staircase occurs at the NATRE site. This suggests that the finger contribution to the vertical buoyancy flux is insufficient for maintaining a series of well-mixed layers and sharp interfaces. If turbulent fluxes produced by shear instability of internal waves are large enough (and frequent enough) to overcome the finger fluxes, the net density flux may be downgradient. Polzin (1996) has found a clear connection between mixing and shear instability at the NATRE site. His work indicates that exceptional dissipation generally occurs when the local Richardson number (Ri = N^2/U_z^2) becomes less than unity. To what extent these turbulent dissipation events compare to the dissipation of salt fingers must be explored further.

Despite the lack of a thermohaline staircase, optical structures recorded during two shadowgraph profiles give qualitative evidence of salt-finger activity. Thin filament-like optical structures (Fig. 3) occurred from the bottom of the mixed layer ($z \sim 150$ m) to the base of the thermocline ($z \sim 1000$ m). These features are most abundant just below the mixed layer, occurring in patches with several meter vertical extent, with gaps between patches of 5–10 m. Patches containing filament structures become more sparse at at greater depth, but generally occur with a frequency of 2–4 patches for every 40 m. While all possible orientations were encountered, filaments in the form of laminae tilted 10°–20° from horizontal were most frequently observed (Fig. 3a). These structures are identical to those previously observed by Kunze et al. (1987) in a thermohaline staircase. As was the case with the staircase observations, the laminae at the NATRE site are characterized by cross-filament wavelengths of 0.5–1 cm. Kunze (1990)
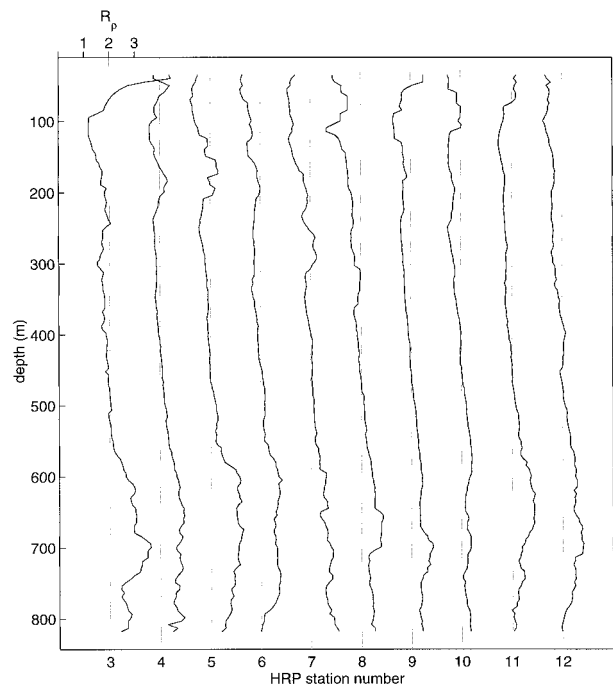
identified these structures as salt fingers that have been tilted by shear. Other classes of optical structures observed include sharp interfaces, isotropic features, and billows.

We regard the abundance of thin tilted laminae at the NATRE site as suggestive evidence for salt fingers. To quantitatively assess the frequency and strength of salt fingers at the NATRE site, we rely on estimates of χ and ϵ derived from HRP microstructure measurements.

3. Quantitative assessment of salt-finger mixing

a. Description of data

Data from the NATRE HRP survey will provide the foundation for this study. However, with the intent of making our study more general, we have supplemented the NATRE data with data from a second HRP survey. These data come from field work conducted in the northeast subtropical Pacific at Fieberling Guyot. Data from the Fieberling survey (TOPO) is discussed by Toole et al. (1997) and Kunze and Toole (1997). In the present study, TOPO data are included as a means of introducing data from a double-diffusively stable (hereafter, doubly stable) stratification regime. While dissipation occurring in the salt-finger regime may be attributable to a combination of turbulence and fingers, dissipation in the
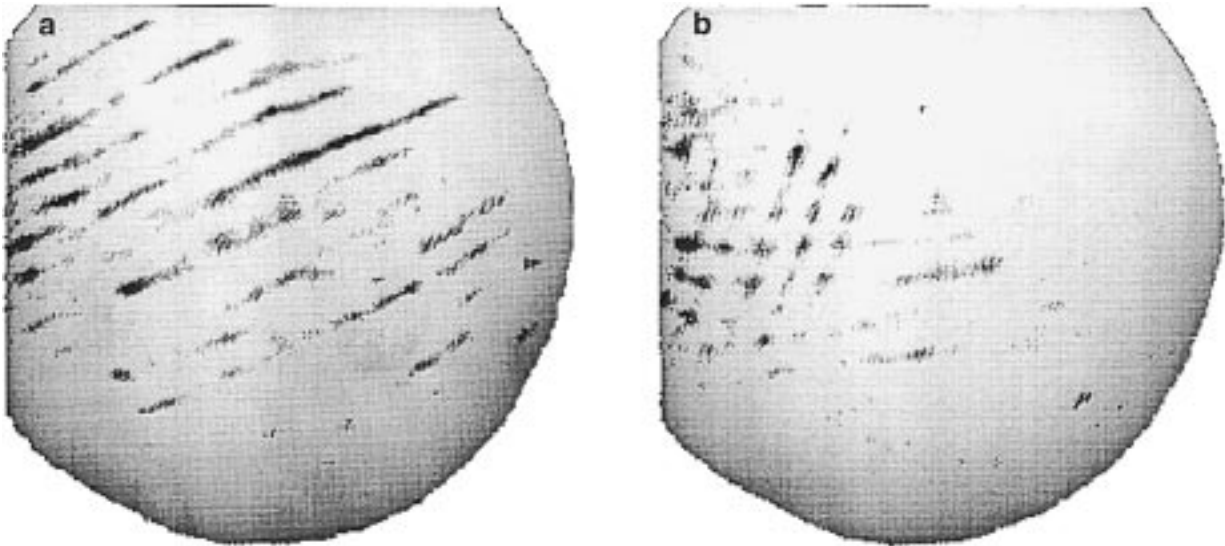
FIG. 3. Shadowgraph images of optical microstructure that were obtained during the NATRE HRP survey. (Shadowgraph image intensity is proportional to the Laplacian of the refractive index of light. The negative of each original image is shown here.) The tilted laminae shown here are observed throughout the thermocline. The circular window has a diameter of 10 cm, and the optical features have a characteristic wavelength of 0.5–1.0 cm. Laminae tilted 10°–20° from the horizontal (a) were the most frequently observed orientation, although filaments with vertical alignment (b) were also observed. The images shown here were obtained near 300-m depth.

doubly stable regime can only be attributed to turbulence. By regarding the features of turbulent dissipation in the doubly stable regime as a null hypothesis, we can objectively assess the dissipation observed in finger-favorable data.

The profile data from NATRE typically extends to 2000 m. These profiles are characterized by a deep mixed layer (80–150 m thick) capping the finger-favorable thermocline. Below the thermocline, intrusive features exist with both ''diffusive'' favorable (the form of double diffusion with cold fresh water over warm salty) and doubly stable character. The TOPO data can be broken into two classes. The data collected above the seamount summit are characterized by high shear and weak stratification in the presence of thermohaline interleaving. The data collected on the seamount flanks are characterized by lower levels of shear and stronger stratification. In particular, these two classes have heterogeneous shear statistics, with shear levels at the summit exceeding those at the flank by a factor of 2. For this reason, we will treat these two classes of TOPO data separately in the analysis that follows. While the stratification at the TOPO site was generally doubly stable, some double-diffusive favorable patches were also present.

Initial processing of all HRP data results in estimates of all conventional (e.g., Θ, S, U, and V) and microstructure quantities at 0.5-m intervals. A detailed description of the algorithms used for this initial stage of data analysis can be found in Polzin and Montgomery (1996). Dissipation rates are calculated from observations of thermal and velocity microstructure using the relations $\chi = 2\kappa(3\overline{\theta_z^2})$ and $\epsilon = \nu(15/4)(\overline{u_z^2} + \overline{v_z^2})$, where κ and ν are the molecular values of thermal diffusion and viscosity. The factor of 3 in the χ expression and the factor of 3.75 in the ϵ expression come from an assumption of small-scale isotropy. Observations supporting the isotropy relations have been made for turbulence (Yamazaki and Osborn 1990) as well as salt fingers (Lueck 1987). Numerical simulations of salt fingers also indicate isotropy for the thermal gradients (Shen 1995). We note that shadowgraph images associated with fingers show significant structural coherence at $O(1$ mm) scales. Since the shadowgraph measures the Laplacian of refractive index, the images tend to emphasize the smallest scales that are mainly influenced by salinity microstructure (Kunze 1990). Thus, small-scale thermal gradients may adhere to the isotropic relationship, while anisotropic salinity structures bias the shadowgraph images.

Finestructure gradient quantities, particularly R_ρ and Ri, will be used extensively in the analysis that follows. To estimate the vertical gradients of scalars, we have used the slope of a linear fit over a 5-m segment, centered at each 0.5-m interval. The 5-m scale was chosen as a suitable trade-off between the need for high vertical resolution and statistically reasonable regression estimation. The magnitudes of all 5-m scalar gradients were compared to their associated standard error. Gradient quantities with standard errors larger than twice their magnitude were excluded from the analysis. This resulted in roughly a 5% data loss, mostly from noisy N^2 estimates. Figure 4 shows typical profiles from the two HRP surveys used for this study. Data from the TOPO survey are shown in Figs. 4a (a seamount summit pro-
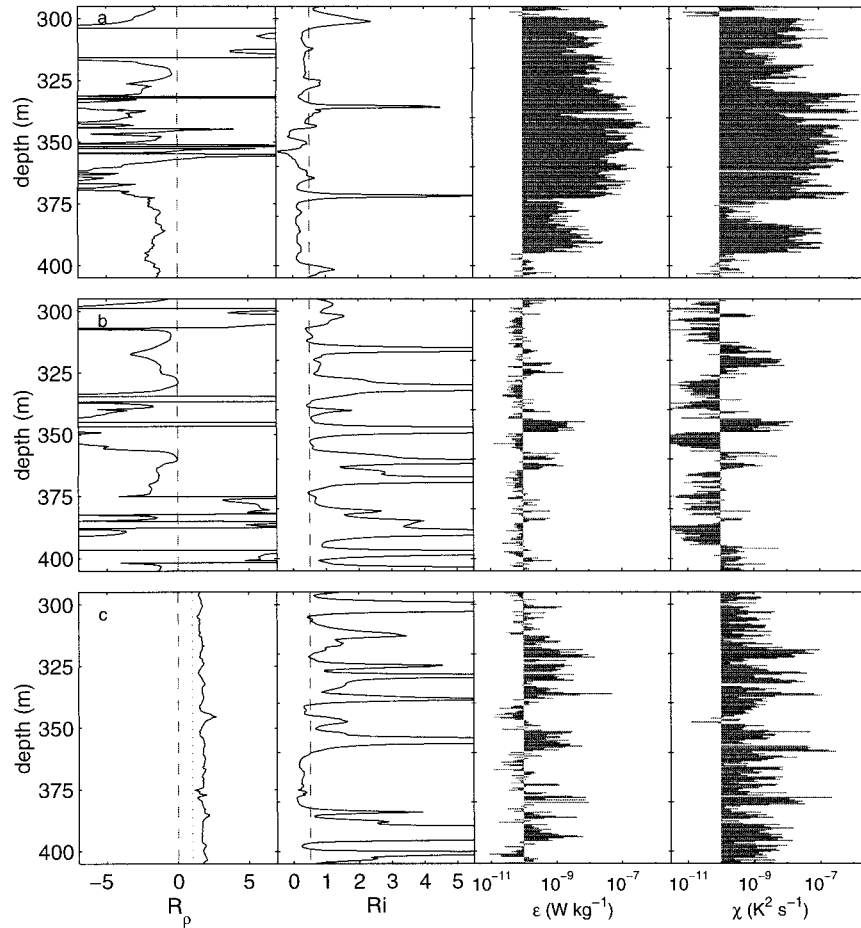
FIG. 4. Characteristic profiles of R_ρ, Ri, ϵ, and χ from the three HRP data groups used in this study. (a) Data from above the summit of Fieberling Guyot collected as part of the TOPO HRP survey. (b) Data from the flank of Fieberling Guyot, about 20 km off the axis of the summit. (c) Data from the NATRE HRP survey. The TOPO site is characterized by predominantly doubly stable stratification ($R_\rho < 0$). In each profile of Ri, a reference value of 0.5 is shown as the dashed vertical line. The high occurrence of low Ri above the seamount distinguishes the summit profiles (a) from those above the seamount flanks (b).

file) and 4b (a seamount flank profile). A profile from NATRE is shown in Fig. 4c.

b. The dissipation ratio model

Mixing by turbulence and salt fingering has traditionally been modeled by the production–dissipation balances for thermal variance (Osborn and Cox 1972) and TKE (Osborn 1980). These balances, in a form relevant to the average over an ensemble of many patches (denoted by $\langle \cdot \rangle$), are given by

$$(1 - R_f)(-k_\rho \langle N^2 \rangle) + R_f \langle \epsilon \rangle = 0, \qquad (1)$$

$$2(-k_\theta \langle \Theta_z \rangle) \langle \Theta_z \rangle + \langle \chi \rangle = 0. \qquad (2)$$

In these expressions, N^2 and Θ_z are the vertical gradients of buoyancy and (potential) temperature, k_ρ and k_θ are the vertical eddy diffusivities of buoyancy and temper-

ature, and R_f is the mixing efficiency. The mixing efficiency, or flux Richardson number, dictates the fraction of Reynolds stress production that is converted to potential energy flux [i.e., $R_f = (-k_\rho \langle N^2 \rangle)/(\langle \overline{u'w'} \rangle \langle U_z \rangle)$].

The buoyancy flux can be written in terms of the fluxes of heat and salt,

$$(-k_\rho \langle N^2 \rangle) = g[\alpha(-k_\theta \langle \Theta_z \rangle) - \beta(-k_s \langle S_z \rangle)]$$
$$= g\alpha(-k_\theta \langle \Theta_z \rangle)(1 - r^{-1}), \qquad (3)$$

where we have used the heat/salt buoyancy-flux ratio $r = (k_\theta/k_s)R_\rho$. In all cases, vertical scalar fluxes have been written in a Fickian form, with the eddy diffusivities being positive for downgradient flux. Furthermore, we have carried a separate diffusivity for each scalar. In the case of salt fingering, not only do we expect the diffusivities to be different, but also that the salt flux can dominate the buoyancy flux so that $k_\rho < 0$.

A general relation involving the ratio of thermal and buoyancy diffusivities can be derived using (1), (2), and (3) with $N^2 = g\alpha\Theta_z(1 - R_\rho^{-1})$,

$$\Gamma = \left(\frac{R_f}{1 - R_f}\right)\frac{k_\theta}{k_\rho} = \left(\frac{R_f}{1 - R_f}\right)\left(\frac{R_\rho - 1}{R_\rho}\right)\left(\frac{r}{r - 1}\right). \quad (4)$$

The nondimensional parameter Γ (Oakey 1985) is the scaled ratio of the dissipation rates

$$\Gamma = \frac{\langle\chi\rangle\langle N^2\rangle}{2\langle\epsilon\rangle\langle\Theta_z\rangle^2}. \quad (5)$$

We will refer to Γ as the "dissipation ratio," although it has been referred to as "the mixing efficiency" by many investigators. While Γ is related to the mixing efficiency, it is more generally related to the ratio of heat and buoyancy diffusivities. Oakey (1985) considered the case of turbulent mixing and derived

$$\Gamma^{(t)} = \frac{R_f}{1 - R_f}. \quad (6)$$

This expression can be obtained from (4) by setting $k_\theta = k_\rho$, so that $r = R_\rho$. The superscript (t) is used to denote that the relation is valid when turbulence is the sole dissipative mechanism. Thus, within the context of turbulent mixing, the dissipation ratio is related in a simple manner to the mixing efficiency R_f. We note that expression (6) can be restated as $\Gamma^{(t)} = (-k_\rho\langle N^2\rangle)/\langle\epsilon\rangle$. Therefore, while R_f is the ratio of potential energy gain to kinetic energy input, $\Gamma^{(t)}$ is the ratio of potential energy gain to kinetic energy loss. Laboratory experiments have demonstrated that the mixing efficiency of turbulence is small, with estimates ranging from $R_f = 0.05$ (Huq and Britter 1995) to $R_f = 0.20$ (Rohr et al. 1984). In terms of the oceanographic application of (1), $\Gamma^{(t)} = 0.2$ is often used (Moum 1996).

Hamilton et al. (1989) and McDougall and Ruddick (1992) considered the case of salt-finger mixing and derived

$$\Gamma^{(f)} = \left(\frac{R_\rho - 1}{R_\rho}\right)\left(\frac{r}{1 - r}\right), \quad (7)$$

with the superscript (f) used to denote dissipation by salt fingers. This expression is also a special case of (4) where the Reynolds stress production $(P = \langle\overline{u'w'}\rangle\langle U_z\rangle)$ is zero such that $\lim_{P\to 0} R_f(1 - R_f)^{-1} = -1$, as is the case for convection with a TKE balance of $(-k_\rho\langle N^2\rangle) = \langle\epsilon\rangle$. Thus, for salt-finger mixing, Γ is (minus) the ratio of the thermal to buoyancy diffusivity (i.e., $\Gamma^{(f)} = -k_\theta/k_\rho$). The size of this ratio is set by both the density ratio and the buoyancy-flux ratio of the fingers. The plausible range of the buoyancy-flux ratio (r) is known from theory (Stern 1975; Schmitt 1979a), laboratory work (Turner 1967; Schmitt 1979b; McDougall and Taylor 1984; Taylor and Bucens 1989), and numerical simulations (Shen 1993, 1995). This collection of work suggests $0.4 < r < 0.7$.

Figure 5 presents the plausible range of the nondimensional parameters of the salt-finger and turbulence models. Results from laboratory studies were used to plot the mixing efficiency of turbulence (5a) and the buoyancy-flux ratio of salt fingers (5b). These numbers were used to compute the dissipation ratio models for turbulence and salt fingers (5c). The value $\Gamma^{(t)} = 0.2$ is shown as representative of the turbulence model, with a plausible range shown as $0.05 < \Gamma^{(t)} < 0.25$. The plausible range of the salt-finger dissipation ratio is shown with a 99% confidence band determined from the density–ratio binned statistics of r.

c. Method of analysis

Our primary investigation of the dissipation rates will be done using the dissipation ratio Γ. The existence of simple models for Γ in cases of turbulent and salt-finger dissipation give this parameter merit. However, two issues detract from this parameter's apparent usefulness. First, differences as small as a factor of 2 distinguish the value of Γ between the two processes. This obstacle can be overcome by incorporating large numbers of dissipation observations into each estimate of Γ to reduce error bars enough to resolve such a subtle parameter range. This is a serious consideration since Γ is the ratio of four noisy variables. Second, given an ensemble of dissipation observations, only a fraction of the data may be representative of mixing events appropriately modeled by (1) and (2). This issue must receive careful attention.

The dissipation rates ϵ and χ are computed by integrating the observed shear and thermal variance residing at scales between about 1 and 50 cm. Variance at these scales originates from diabatic, irreversible processes. The processes of turbulence and salt fingering are among these, producing fluxes of heat, salt, and buoyancy that irreversibly alter the local temperature, salinity, and density fine structure. However, it is plausible that internal wave and molecular processes may also account for variance at small enough scales to influence dissipation estimates, and these set the oceanic background levels of the dissipation rates. This type of oceanic "noise" is not appropriately modeled by (1) and (2). Similarly, the noise of the sensors and associated electronics, though low for the HRP (Polzin and Montgomery 1996), will contribute to uncertainty in ϵ and χ.

In the work presented here, we seek to attribute observations of irreversible microstructure to salt fingers or turbulence. We have attempted to rule out the influence of noisy dissipation estimates by only examining dissipative events of higher magnitude, while still retaining enough data to uncover a potentially subtle signal of salt fingers. To do this, we have used the combined dataset involving observations from both NATRE and TOPO surveys. This combined dissipation record was then examined in terms of various upper thresholds of dissipation rate magnitude, this being done separately
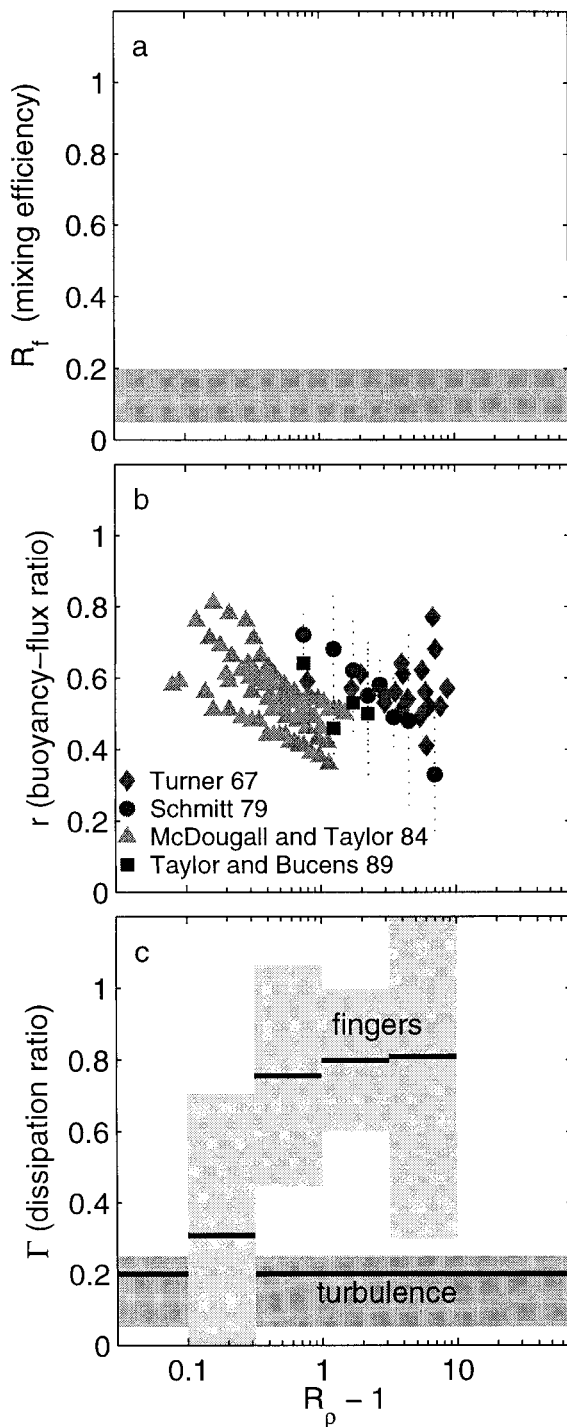
FIG. 5. The plausible range of three nondimensional parameters for finger-favorable stratification ($R_\rho > 1$). The logarithmic axis for $R_\rho - 1$ is useful because the distribution of finger-favorable R_ρ is approximately lognormal about $R_\rho = 2$. (a) The mixing efficiency of turbulent mixing (R_f). Laboratory data supports the range $0.05 < R_f < 0.20$. (b) The buoyancy-flux ratio of salt fingers (r) from laboratory data. (c) The range of the dissipation ratio for turbulence and salt fingers are shown. The turbulence model was calculated using $\Gamma^{(t)} = R_f(1 - R_f)^{-1}$, with $\Gamma^{(t)} = 0.2$ taken as the nominal value. The finger model was computed from the laboratory data for r, with average values of r binned by R_ρ. The 99% confidence band is shown for the finger model, while the range for the turbulence model is dictated by $0.05 < R_f < 0.20$.

for observations occurring in doubly stable and finger-favorable patches.

We have found that exceptional levels of finger-favorable χ are associated with bimodal ϵ statistics. In particular, we have examined the distribution of ϵ data using a threshold defined as $\chi > \chi_{75} \sim 1 \times 10^{-9}$ K^2 s^{-1}: the upper 75th percentile of the combined χ record. The statistical distribution for $\epsilon(\chi > \chi_{75})$ is shown in Fig. 6. The finger-favorable data (Fig. 6a) seems to have a primary mode at $\epsilon \sim 2 \times 10^{-10}$ W kg^{-1}, with the secondary mode occurring near $\epsilon \sim 1 \times 10^{-9}$ W kg^{-1}. A simple statistical test for bimodality (Haldane 1952) indicates that the apparent antimode at $\epsilon \sim 5 \times 10^{-10}$ W kg^{-1} is significant to the 0.15 level (i.e., significant at the 85% confidence level). In contrast to the finger-favorable data, the associated distribution of doubly stable ϵ data lacks bimodal character (Fig. 6b). Both turbulence and salt fingers act as dissipative mechanisms in the finger-favorable regime, while only turbulence acts in the doubly stable regime. The existence of bimodal ϵ in only the finger-favorable regime suggests that the two modes are associated with the two processes.

To investigate the character of the finger-favorable data more thoroughly, we have examined the $\epsilon(\chi > \chi_{75})$ population in terms of the stability parameters R_ρ and Ri. Figure 7 shows the distribution of $\epsilon(\chi > \chi_{75})$ data after being partitioned into four subsections of (R_ρ, Ri) data space. When the portion of parameter space having Ri > 1 is considered, the low-ϵ mode dominates. This is particularly true when $R_\rho < 2$ (Fig. 7a), this low density ratio range having about twice the number of $\chi > \chi_{75}$ events as $R_\rho > 2$ (Fig. 7b). In the portion of parameter space with Ri < 1 (Figs. 7c and 7d), the high-ϵ mode is apparent at both large and small values of R_ρ. However, in the case where ($1 < R_\rho < 2$, Ri < 1), a low-ϵ mode is also apparent, with a population comparable to the high-ϵ mode. The documented trend is consistent with an association of the two modes with turbulence and salt fingering. In particular, we associate the low-ϵ mode, dominant at low R_ρ, with salt fingers. We associate the high-ϵ mode, dominant at low Ri, with turbulence.

Ruddick et al. (1997) used microstructure observations from a different instrument to examine dissipation at the NATRE site. The noise level of their measurements limited their analysis to observations having $\epsilon > 7 \times 10^{-9}$ W kg^{-1} Their observations clearly fall into the high-ϵ mode that we have associated with turbulence. Ruddick et al. (1997) use a Reynolds number Re $= \epsilon/(\nu N^2)$, and they find no clear evidence of salt fingers in the parameter range $10^1 < $ Re $ < 10^4$. In a salt-finger regime, the parameter $\epsilon/(\nu N^2)$ is equivalent to the Stern number $J_b/(\nu N^2)$. Stern (1969) argued that this parameter must be $O(1)$ for fingers to be active, while McDougall and Taylor (1984) found experimentally that the Stern number can be $O(10)$ for $R_\rho < 2$. A characteristic Stern number for our low-ϵ mode is $O(10)$. Thus,

finger–favorable dissipation
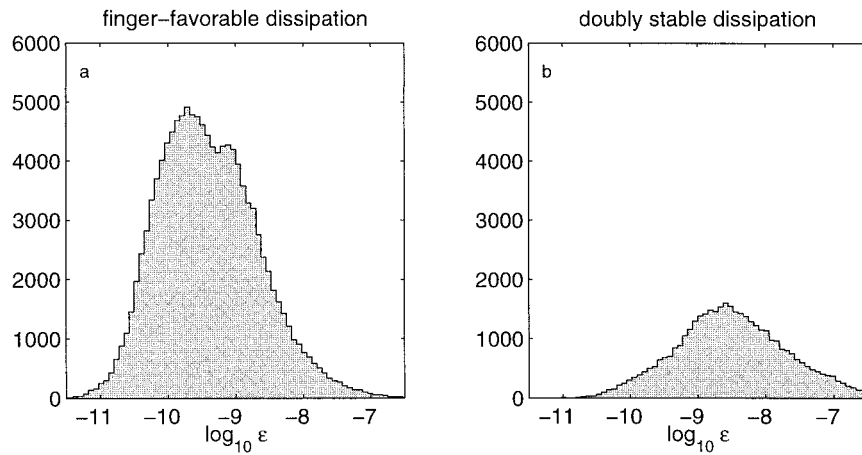
doubly stable dissipation

FIG. 6. Histogram of the TKE dissipation rate for the subset of observations having $\chi > \chi_{75}$ for (a) all finger-favorable data and (b) all doubly stable data. The upper quartile of the combined TOPO and NATRE thermal dissipation record is $\chi_{75} \sim 1 \times 10^{-9}$ K^2 s^{-1}. The bimodal structure in the finger-favorable histogram is statistically significant at the 0.15 level. The modes are located at $\epsilon \sim 2 \times 10^{-10}$ W kg^{-1} and $\epsilon \sim 1 \times 10^{-9}$ W kg^{-1}.

$1 < R_\rho < 2, 1 < Ri < \infty$

$2 < R_\rho < \infty, 1 < Ri < \infty$

$1 < R_\rho < 2, 0 < Ri < 1$

$2 < R_\rho < \infty, 0 < Ri < 1$
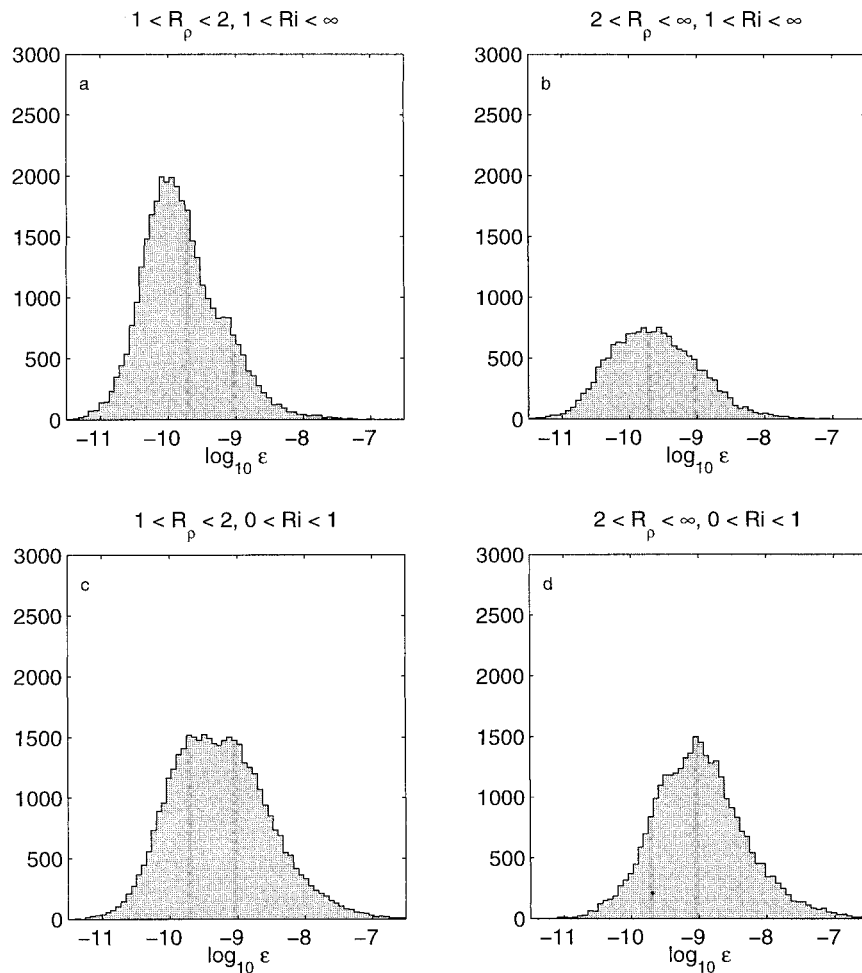
FIG. 7. The finger-favorable distribution of $\epsilon(\chi > \chi_{75})$ is broken into four distinct regions of (R_ρ, Ri) data space. In each histogram, the ϵ bins corresponding to the modes of the distribution shown in Fig. 6a are emphasized by darker shading.

the Ruddick et al. (1997) Reynolds numbers are too large to admit the possibility for fingers.

In examining only an upper threshold of our dissipation data, we have attempted to filter out weak dissipation events not likely associated with salt fingers or turbulence, as well as those sites where signals are weak relative to instrumental noise levels. Additionally, we will assume that a subset of observations with $\chi > \chi_{75}$ can be well modeled by the production–dissipation balances of (1) and (2). In doing so, we will expect the dissipation ratio analysis of this data to provide valuable information on the mixing processes to which the dissipation is attributable. By examining Γ in the (R_ρ, Ri) parameter space, we may capitalize on the association between the two dissipative processes and their stability parameters. We expect Γ to be consistent with the turbulence model at low Ri and with the salt-finger model at low (finger favorable) values of R_ρ. There are regions of the (R_ρ, Ri) parameter space that do not favor either process. These include the large Ri region of the doubly stable regime, and the region of the finger-favorable regime where both Ri and R_ρ are large. In these regions where the finger and shear instabilities are not favored, exceptional dissipative events should be rare.

d. Statistical treatment of dissipation data

Mean and variance estimation of dissipation rate data has been discussed by many authors. The apparent tendency for the statistical distributions of χ and ϵ to be lognormal has produced arguments in favor of maximum likelihood estimation (MLE; Baker and Gibson 1987). The breakdown of lognormality assumptions has also been documented, and Davis (1996) concludes that arithmetic estimation is the most robust form of analysis. Also, we have evaluated the different estimation methods through Monte Carlo exercises involving lognormally distributed random data. For random data distributions with characteristics reflecting those of our dissipation data, the discrepancy between MLE and arithmetic methods becomes less than 10% for as few as 200 degrees of freedom. For these reasons, arithmetic estimation was adopted as the analysis procedure for this study.

To compute estimates of $\Gamma(R_\rho, \mathrm{Ri})$, ensemble averages were computed for all data within a discrete bin of (R_ρ, Ri) parameter space. The standard error of Γ within the bin was computed as

$$\delta\Gamma = \frac{\Gamma}{\sqrt{n}}\left[\left(\frac{\delta\epsilon}{\langle\epsilon\rangle}\right)^2 + \left(\frac{\delta\chi}{\langle\chi\rangle}\right)^2 + \left(\frac{\delta N^2}{\langle N^2\rangle}\right)^2 + \left(\frac{2\delta\Theta_z}{\langle\Theta_z\rangle}\right)^2 \right.$$
$$\left. - \frac{2\sigma^2}{\langle N^2\rangle\langle\Theta_z\rangle}\right]^{1/2}, \tag{8}$$

where the $\delta(\cdot)$ terms appearing in the parenthesis are the standard deviations, σ^2 is the covariance of N^2 and Θ_z, and n is the number of degrees of freedom of the

data in the bin. The derivation of (8) follows standard error propagation methods (Bevington and Robinson 1992). Degrees of freedom in the 0.5-m ϵ and χ data were estimated using a vertical-lag correlation analysis. This was done for each of the datasets, with TOPO seamount summit data being treated separately from the seamount flank data. The NATRE dissipation profiles were characterized by correlation scales (vertical separation scales) of 5 m in the thermocline ($z < 800$ m) and 10 m at greater depths. TOPO dissipation profiles were characterized by large correlation scales, generally around 20 m for both seamount summit and flank profiles. A single degree of freedom is represented by the grouping of 0.5-m data within one correlation scale in a single profile. For the ensemble of data in each bin, the number of such groupings gives the total degrees of freedom.

e. Results

We begin our examination of exceptional dissipation data within the doubly stable regime. The available datasets were subsampled in favor of all 0.5-m dissipation observations with corresponding density ratio in the doubly stable range $-100 < R_\rho < -1$. Data in the density ratio range between -1 and 0 were held from the analysis, as these data are characterized by weak thermal stratification where $\Theta_z \to 0$, making $\Gamma \propto N^2/\Theta_z^2$ singular. The data were assigned into a (R_ρ, Ri) data space by first selecting a bulk class of Ri, and then subdividing the particular Ri population into bins of R_ρ. Bins of R_ρ were each chosen to have 1000 elements of the 0.5-m data. In this way, each R_ρ bin generally contained 200–500 degrees of freedom. The mean and standard error of Γ in each bin were then calculated using (5) and (8).

Analysis of the exceptional doubly stable dissipation data is shown in Fig. 8. The data were classified into six overlapping populations of Ri. In each panel, the symbol and error bar denote the mean with 95% confidence interval for a 1000-element bin of data, with the symbol centered at the bin's mean density ratio. Richardson numbers less than 1 are considered in Figs. 8a, 8b, and 8c. These data are characterized by Γ between 0.1 and 0.25, in good agreement with the results of previous studies (Moum 1996; Ruddick et al. 1997). Additionally, Γ has no discernible density ratio dependence. We note that 75% of all exceptional dissipation data within the doubly stable regime occur when Ri < 1. The 25% of exceptional TOPO χ data that occur in patches where Ri > 1 are shown in Figs. 8d, 8e, and 8f. Data at Ri > 5 are too sparse to yield a single 1000-element estimate. However, available data occurring at Ri > 1 show Γ between 0.15 and 0.25, numbers like those observed at lower values of the Richardson number.

Exceptional dissipation occurring in the finger-favorable regime was investigated by conditionally sam-
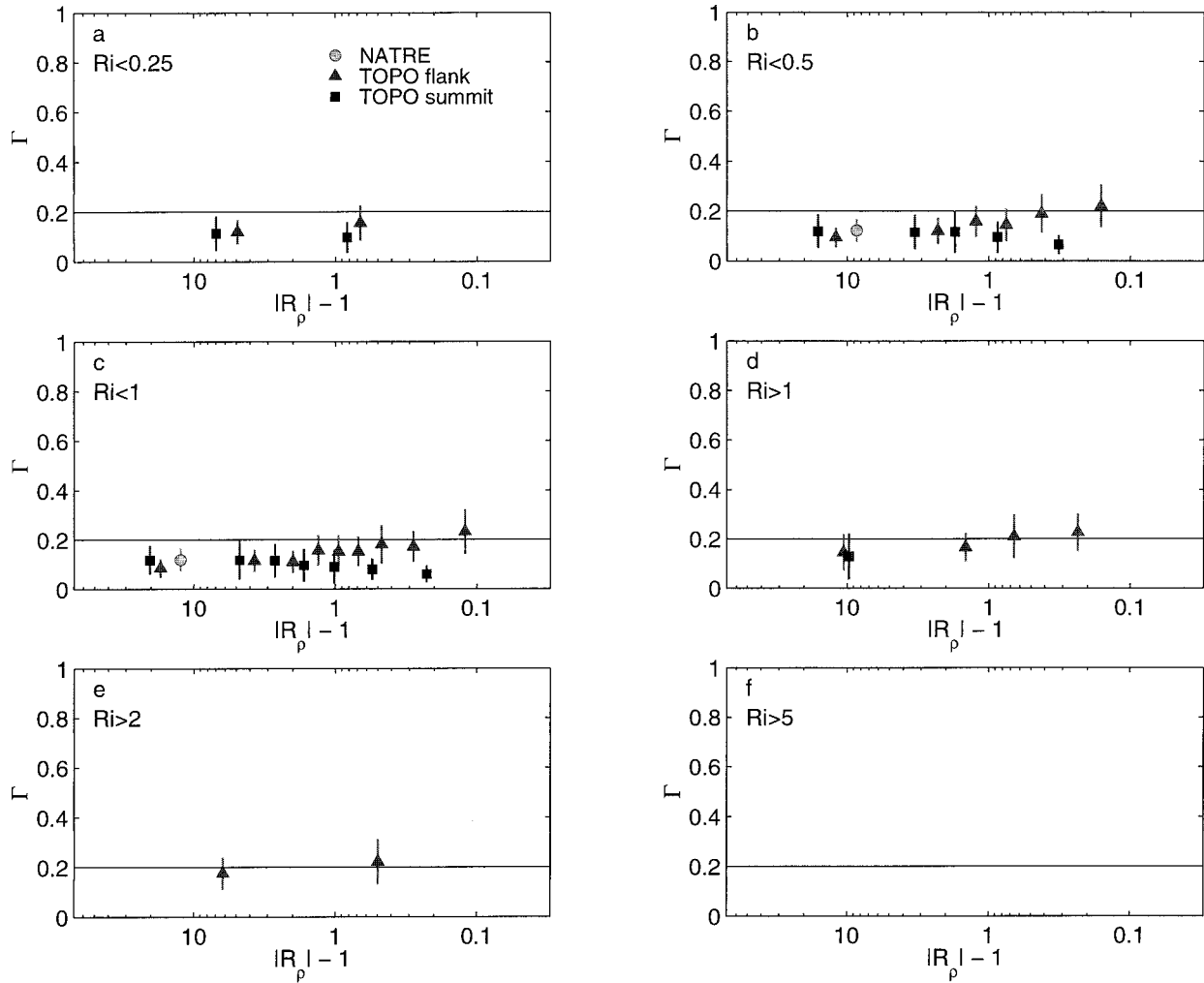
FIG. 8. The dissipation ratio of doubly stable observations with $\chi > \chi_{75}$. The data were grouped into six different Ri populations (a)–(f). Estimates were derived separately for each of the three HRP data groups: NATRE (circles), TOPO seamount flank (triangles), and TOPO seamount summit (squares). Each symbol is the estimate $\Gamma = (\langle N^2 \rangle \langle \chi \rangle)(2\langle \epsilon \rangle \langle \Theta_z \rangle^2)^{-1}$, where the ensemble average was computed for a bin of 1000 dissipation estimates. The error bars give the 95% confidence interval for a reduced number (<1000) of degrees of freedom. In each panel, a reference value of $\Gamma = 0.2$ is shown.

pling the available data for patches with $R_\rho > 1$. As was done for the doubly stable data, these data were conditionally sampled into six overlapping populations of Ri and then sorted by R_ρ in bins of 1000 elements. Data from the NATRE survey contributes most of the finger-favorable observations, with bins containing 400–700 degrees of freedom.

For finger-favorable observations with Ri < 1 (Figs. 9a–c), Γ occupies the range of values exhibited by the doubly stable data, $0.1 < \Gamma < 0.3$. However, there is an elevation of Γ at larger values of the Richardson number, consistent with expectations of salt fingers. To assess the significance of the observed trend in Γ at large Ri within the context of salt-finger mixing, we can use (7) to give an expression for r in terms of Γ,

$$r = \frac{R_\rho \Gamma^{(f)}}{R_\rho \Gamma^{(f)} + R_\rho - 1}. \tag{9}$$

Using this relation, we have compared the Ri > 5 NATRE data (Fig. 9f) with the results of laboratory salt-finger observations, theoretical relations, and a numerical simulation (Shen 1993). This comparison is shown in Fig. 10. Only the McDougall and Taylor (1984) experiments consistently achieved the low-density ratio range most relevant for comparison with the NATRE data. The NATRE data dictate a buoyancy-flux ratio in the range $0.6 < r < 0.7$ for density ratios less than 1.6. Lower flux-ratio values of $0.4 < r < 0.5$ are inferred for $R_\rho \sim 2$. The range of r values exhibited by the NATRE data is consistent with the laboratory data, not-
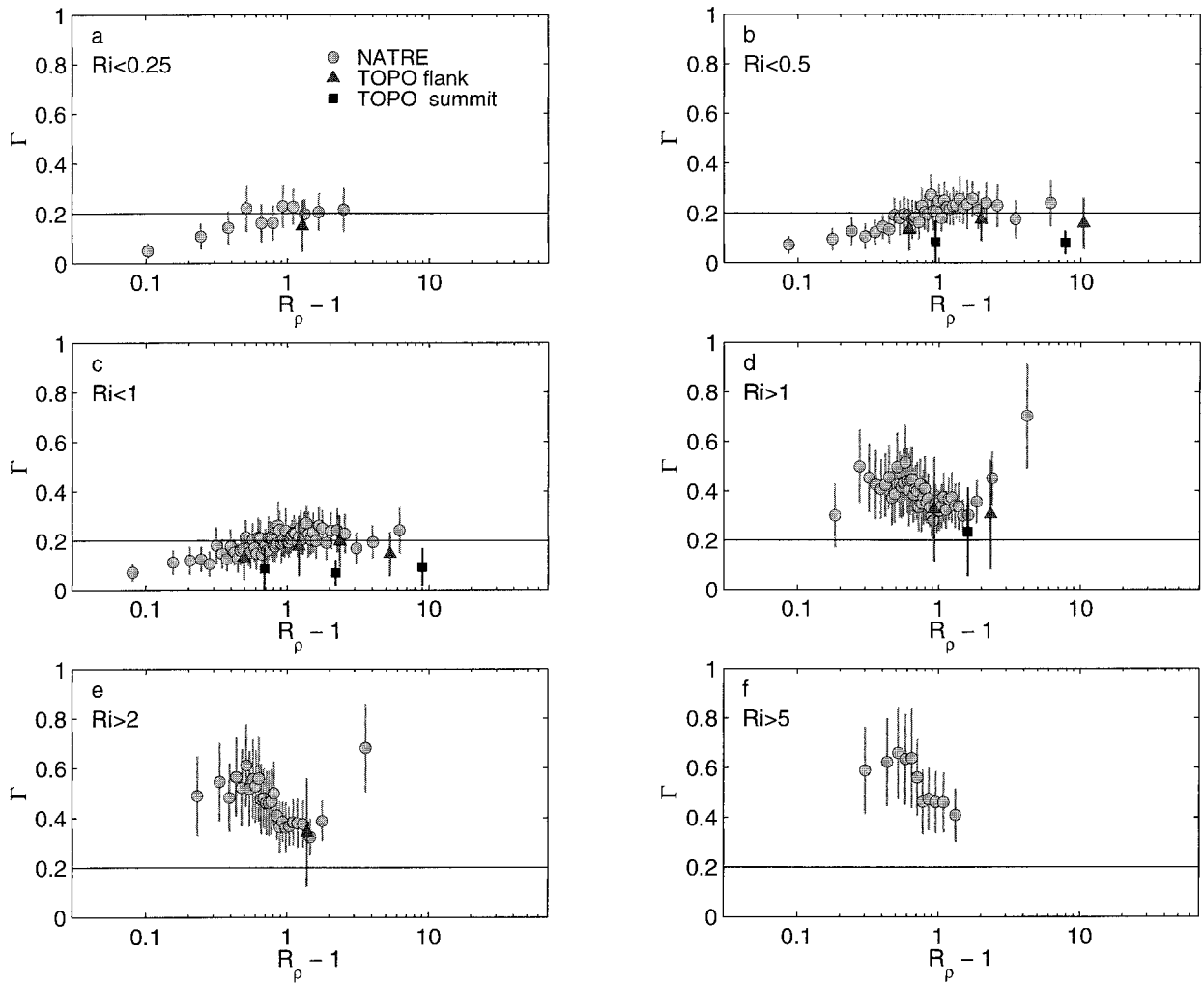
FIG. 9. The dissipation ratio of finger-favorable observations with $\chi > \chi_{75}$.

ing that the r values reported at $R_\rho = 1.75$ by Schmitt (1979b) and Taylor and Bucens (1989) are the summaries for measurements made at density ratios as low as $R_\rho = 1.6$. In particular, the NATRE data suggest a decline in flux ratio, also observed by McDougall and Taylor, as R_ρ goes from 1 to 2.

A formal statistical examination of the dissipation ratio signal was done after assembling a gridded (R_ρ, Ri) data space for both doubly stable and finger-favorable regimes. As in the analysis described above, we have selected data from the upper quartile χ population of the combined TOPO and NATRE dataset. This data space consisted of discrete data bins uniformly spaced in the set of transformed coordinates [log($|R_\rho| - 1$), log(Ri)]. This choice of coordinates is favorable because it maps a wide range of parameter values, while emphasizing the parameter range ($R_\rho < 2$, Ri < 1) where most of the data lies. Figure 11 shows contour maps of Γ for both stratification regimes. The shaded bins in each map contain 100 or more degrees of freedom. Bins

with fewer degrees of freedom were excluded from the analysis. We find that the doubly stable regime is well characterized by a constant value of the dissipation ratio of $\Gamma = 0.16 \pm 0.04$. In contrast, while much of the finger regime is characterized by $0.2 < \Gamma < 0.3$, elevated values of Γ dominate the upper left (small R_ρ, large Ri) quadrant of the map.

To evaluate the significance of the finger-regime results, we have implemented a simple statistical test. The dissipation ratio result from the doubly stable regime is taken as indicative of turbulent mixing. Specifically, we take $\Gamma^{(t)} = 0.16 \pm 0.04$ as the null hypothesis of mixing attributable to turbulence. We have tested the finger-regime results against this null hypothesis, seeking evidence that the dissipation ratio estimates of the finger-favorable data are different from those of the doubly stable data. The results of the two-tailed hypothesis test are shown in Fig. 12a. The standardized variable $Z = (\Gamma - \Gamma^{(t)})(\delta\Gamma^2 + \delta\Gamma^{(t)2})^{-1/2}$ was tested at the 0.01 significance level. The null hypothesis of $\Gamma = \Gamma^{(t)}$ is ac-
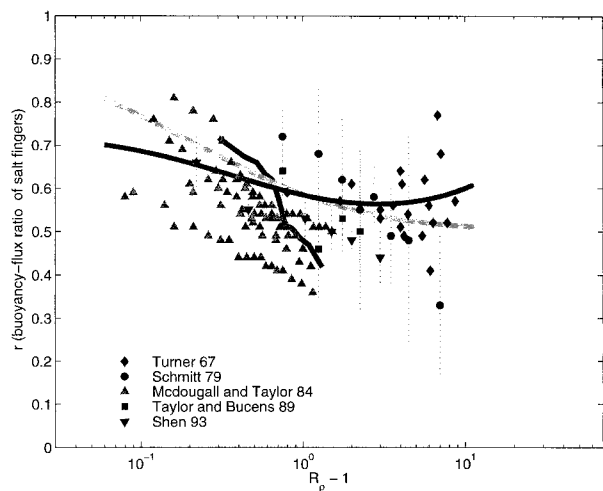
FIG. 10. Estimates of the salt finger buoyancy-flux ratio $r = (\alpha k_\theta \Theta_z)(\beta k_s S_z)^{-1}$. The results of four laboratory experiments are shown: Turner (1969, diamonds), Schmitt (1979b, circles), McDougall and Taylor (1984, upward triangles), and Taylor and Bucens (1989, squares). Also shown are the numerical results of Shen (1993, downward triangles) and the theoretical models of Stern (1975, light curve), and Schmitt (1979a, dark curve). Buoyancy-flux ratio estimates were derived from HRP observations by assuming that the NATRE ($\chi > \chi_{75}$, Ri > 5) dissipation ratio signal (Fig. 9f) was entirely attributable to salt fingers. The relation $r = R_\rho \Gamma (R_\rho \Gamma + R_\rho - 1)^{-1}$ was used. The HRP data-derived estimates are shown with a 99% confidence band.

cepted in nearly all of quadrants—I, III, and IV—of the finger-favorable regime. However, the data in quadrant II ($R_\rho < 2$, Ri > 1) strongly supports the alternate hypothesis $\Gamma \neq \Gamma^{(t)}$. A second statistical test was used to evaluate the possibility of salt-finger mixing. The finger model was evaluated using the laboratory r data (Fig. 5b), and the null hypothesis of $\Gamma = \Gamma^{(f)}$ was tested at the 0.01 significance level using the test variable $Z = (\Gamma - \Gamma^{(f)})(\delta\Gamma^2 + \delta\Gamma^{(f)2})^{-1/2}$. Subject to this test, all of the data in quadrant II meets consistency with the finger model (Fig. 12b). As is apparent after comparing Figs. 12a and 12b, a small class of data is consistent with both models for the dissipation ratio. This degenerate class of data is the result of (i) the overlap of the $\Gamma^{(t)}$ and $\Gamma^{(f)}$ models when $R_\rho < 1.4$ and (ii) bins having large values of $\delta\Gamma$. In classifying this degenerate data, we have given preference to the turbulence model. Thus, we attribute the dissipation ratio signal to turbulence in nearly all of quadrants—I, III, and IV—while quadrant II is associated with fingers. This resulting classification is shown in Fig. 12c along with the percentage of observations represented in each bin. Through the application of these two tests, we have classified all but 1% of our $\chi > 1 \times 10^{-9}$ K^2 s^{-1} data as either attributable to turbulence or salt fingers.

By testing the original null hypothesis of turbulence at the 0.01 significance level, we have allowed for very generous uncertainty in the value of $\Gamma^{(t)}$. This also makes the rejection of the null hypothesis very difficult. In this manner we have been very conservative in labeling any binned $\chi > \chi_{75}$ data as "nonturbulence." Similarly, by
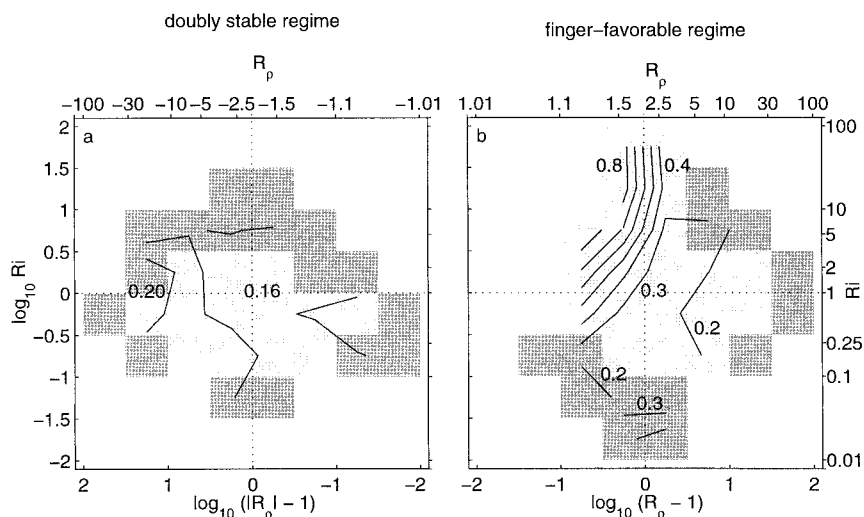

FIG. 11. A contrast between $\Gamma(R_\rho, \text{Ri})$ of doubly stable and finger-favorable exceptional χ observations. Observations were grouped into bins of the [$\log(|R_\rho| - 1)$, $\log(\text{Ri})$] parameter space, and Γ was estimated in bins where the data density exceeded 100 degrees of freedom (all shaded regions). In each panel, the estimate $\Gamma = (\langle N^2 \rangle \langle \chi \rangle)(2 \langle \epsilon \rangle \langle \Theta_z \rangle^2)^{-1}$ is contoured. Regions of darker shading denote bins where the uncertainty of Γ exceeds 25% of the mean. The doubly stable regime (a) is characterized by a broad parameter range having $\Gamma = 0.16$ (inner three contours). The finger-favorable regime (b) is characterized by larger values of Γ, particularly in the (low R_ρ, large Ri) region of parameter space [quadrant II, ($R_\rho < 2$, Ri > 1)].
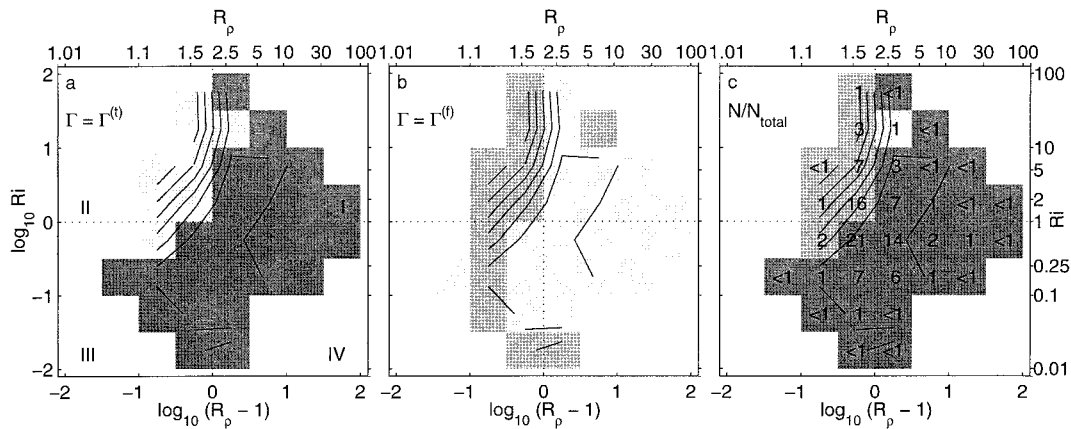
FIG. 12. Statistical classification of the exceptional χ observations in the finger-favorable regime. (a) The observations were tested against the null hypothesis that Γ was attributable to turbulence. The finger-favorable regime can be broken into the four quadrants defined by the [log($R_\rho - 1$), log(Ri)] data space (I–IV as labeled). Most of quadrants I, III, and IV are consistent with the turbulence hypothesis at the 0.01 significance level (99% confidence), and these bins are identified by dark shading. (b) The observations were tested against the null hypothesis that Γ was attributable to salt fingers. Data consistent with the finger hypothesis are indicated by dark shading. All of the quadrant II data meet consistency with the finger model at the 0.01 significance level, as do several bins already found to be consistent with turbulence. (c) The percentage of total data represented by each bin is reported. Those data with degenerate classification are assigned to turbulence. This results in the classification of nearly 70% of the data as turbulence (darkest shading) and 30% as salt fingers (medium shading). $N_{total} = 119\ 570$.

testing the "nonturbulent" observations against a salt-finger hypothesis at the 0.01 significance level, we have allowed generous uncertainty in the $\Gamma^{(f)}$ model. For these reasons, we view this work as a consistency check. The upper quartile of χ observations having stability parameters in the range ($R_\rho < 2$, Ri > 1) can be attributed to salt fingers in a manner consistent with available information from theory and laboratory work.

4. Mixing at the NATRE site

a. Vertical mixing influenced by salt fingers

We seek estimates of the net diffusivities k_θ and k_s that dictate the vertical fluxes over $O(100\ m)$ scales. In such estimates, the presence of salt-finger mixing will tend to enhance the haline diffusivity over the thermal diffusivity. Since there is a high occurrence of patches with low R_ρ and stable Ri at the level of the tracer injection in NATRE, we find much of the dissipation can be ascribed to salt fingers.

To derive estimates of the net diffusivities, we employ 100 uniformly spaced stations from a 400 km × 400 km survey grid (Fig. 1). This April 1992 survey took 18 days to complete. Each profile includes a full record of dissipation data to 2000 m. Our goal is to estimate survey scale diffusivities applicable to the synoptic snapshot represented by our survey. We make the assumption that the variance budgets (1) and (2) are valid within the context of (i) survey scale lateral averaging, (ii) $O(100\ m)$ vertical averaging, and (iii) the time average invoked by treating the 18-day survey as a snapshot.

The mean field was derived with reference to a neutral-density coordinate system (σ_n; Jackett and McDougall 1997). Epineutral (i.e., along neutral surface) averaging yielded mean profiles of $\overline{\Theta}$ and $\overline{S}$ in terms of a vertical coordinate $\overline{z}$, the mean depth of each density surface. All mean field variables are associated with some uncertainty. In the case of $\overline{\Theta}$ and $\overline{S}$, standard errors as large as $\delta\overline{\Theta} = 0.02$ K and $\delta\overline{S} = 0.005$ (values typical of the 100-m deep neutral surface) can be ascribed to mesoscale eddies. The uncertainty in the mean vertical coordinate $\overline{z}$ is more limiting, with $\delta\overline{z} = 5$ m. The variability associated with $\overline{z}$ is attributable to large-amplitude internal tides. Mean vertical gradient quantities ($\overline{\Theta}_z$, $\overline{S}_z$, and $\overline{N^2}$) were calculated from $O(100\ m)$ linear fits to $\overline{\Theta}(\overline{z})$ and $\overline{S}(\overline{z})$. The dominant uncertainty in the vertical gradients comes from $\delta\overline{z}$, yielding a 2% error in the $\overline{N^2}$ estimates.

The vertical diffusivities k_θ and k_s were calculated using a scheme that follows from the results of our (R_ρ, Ri) analysis of Γ. The general form of the model we will employ has similarities to the model suggested by McDougall and Ruddick (1992). The differences between our approach and that of McDougall and Ruddick (1992) will be described in section 5. Our approach is motivated by the results of the dissipation ratio analysis of exceptional χ data (section 3e). Within each layer, all dissipation data are partitioned into two groups. All 0.5-m ϵ and χ estimates associated with ($1 < R_\rho < 2$, Ri > 1) are presumed salt-finger dissipation. All dissipation associated with R_ρ and Ri outside the finger-favorable range [i.e., the complement of ($1 < R_\rho < 2$, Ri > 1)] are attributed to turbulence. In this manner, we attribute some percentage of the dissipation obser-

TABLE 1. Net diffusivity estimates.

$\overline{z}$ (m)	$\overline{R_\rho}$	$P^{(f)}$	$P^{(t)}$	k_θ (cm^2 s^{-1})	k_s (cm^2 s^{-1})	k_ρ (cm^2 s^{-1})
90	1.63	0.10	0.90	0.93 $\pm$ 0.19	1.22 $\pm$ 0.25	0.48 $\pm$ 0.63
190	1.65	0.44	0.56	0.12 $\pm$ 0.02	0.22 $\pm$ 0.03	-0.03 ± 0.06
300	1.71	0.48	0.52	0.08 $\pm$ 0.01	0.13 $\pm$ 0.01	0.01 $\pm$ 0.03
400	1.91	0.35	0.65	0.07 $\pm$ 0.01	0.10 $\pm$ 0.01	0.03 $\pm$ 0.03
500	2.16	0.09	0.91	0.07 $\pm$ 0.01	0.08 $\pm$ 0.01	0.06 $\pm$ 0.03
600	2.46	0.05	0.95	0.06 $\pm$ 0.01	0.07 $\pm$ 0.01	0.05 $\pm$ 0.02
700	2.53	0.08	0.92	0.06 $\pm$ 0.01	0.09 $\pm$ 0.01	0.04 $\pm$ 0.02
800	2.57	0.10	0.90	0.07 $\pm$ 0.01	0.12 $\pm$ 0.02	0.04 $\pm$ 0.02

vations to fingers ($P^{(f)}$) and turbulence ($P^{(t)} = 1 - P^{(f)}$). In using this approach, we assume that the regime partition found for exceptional χ is more generally applicable to the ensemble averages of dissipation profiles. We will further discuss the applicability of this model in section 5.

Diffusivities in each layer are first calculated for the two dissipative regimes. In the case of turbulent dissipation, we use the Osborn (1980) diffusivity model,

$$k_0^{(t)} = \Gamma^{(t)} \langle \epsilon \rangle^{(t)} (\overline{N^2})^{-1}, \qquad (10)$$

where $\langle \epsilon \rangle^{(t)}$ denotes the ensemble average of the ϵ identified as attributable to turbulence, and $\Gamma^{(t)}$ is the dissipation ratio for turbulence. We take $k_0^{(t)}$ as the diffusivity for both heat and salt. In these calculations, we use $\Gamma^{(t)} = 0.2$, the value consistent with most previous work. The standard error of the turbulence diffusivity is also calculated,

$$\delta k_0^{(t)} = k_0^{(t)} \left[\left(\frac{\delta\Gamma^{(t)}}{\Gamma^{(t)}} \right)^2 + \left(\frac{\delta\langle\epsilon\rangle^{(t)}}{\langle\epsilon\rangle^{(t)}} \right)^2 + \left(\frac{\delta\overline{N^2}}{\overline{N^2}} \right)^2 \right]^{1/2}, \quad (11)$$

We have calculated $\delta\langle\epsilon\rangle^{(t)}$ using a bootstrap method (Efron and Gong 1983). The number of degrees of freedom in the bootstrap estimates were determined from the number of nonoverlapping 5-m profile segments in the ensemble. For the uncertainty of the turbulent dissipation ratio, we have used the result of our doubly stable data analysis, $\delta\Gamma^{(t)} = 0.04$ (Fig. 11a). In the case of salt-finger dissipation, we use the Osborn and Cox (1972) diffusivity model,

$$k_\theta^{(f)} = 0.5\langle\chi\rangle^{(f)}(\overline{\Theta_z^2})^{-1}, \qquad (12)$$

where $\langle\chi\rangle^{(f)}$ denotes the ensemble average of the χ observations identified with salt fingers. The haline diffusivity is then calculated through use of the buoyancy-flux ratio of fingers $r = (\alpha k_\theta^{(f)}\overline{\Theta}_z)(\beta k_s^{(f)}\overline{S}_z)^{-1}$. Thus,

$$k_s^{(f)} = \frac{\overline{R_\rho}}{r} k_\theta^{(f)}, \qquad (13)$$

where $\overline{R_\rho}$ is the density ratio computed from the $O(100$ m) scale vertical gradients. (We note that $\overline{R_\rho}$ is not necessarily equal to the ensemble average of localized 5-m R_ρ estimates.) In (13) we use a buoyancy-flux ratio of $r = 0.6 \pm 0.04$, a value taken from the $1.5 < R_\rho < 2$ laboratory data (Fig. 10). The net diffusivities for each

layer are then calculated as the weighted average of the regime-based diffusivities

$$k_\theta = P^{(t)} k_0^{(t)} + P^{(f)} k_\theta^{(f)}, \qquad (14a)$$

$$k_s = P^{(t)} k_0^{(t)} + P^{(f)} k_s^{(f)}. \qquad (14b)$$

Thus, the net diffusivities depend on both the frequency and magnitude of the salt-finger and turbulent dissipation events. For a profile with no finger-favorable mixing ($P^{(f)} = 0$), both diffusivities converge to the value $k_0^{(t)}$.

Estimates of net diffusivities for each layer, as well as the weighting factors $P^{(f)}$ and $P^{(t)}$, are given in Table 1. Figure 13 presents a summary of these results. Density ratio information is given in Fig. 13a. For each layer, the median value of the 5-m R_ρ is shown as a vertical line. The density ratio range encompassed by the lower and upper quartile is also shown, as indicated by the shaded band within each layer. The density ratio calculated for the 100-m scale density ratio ($\overline{R_\rho}$) is also shown. We note that $\overline{R_\rho}$ is generally close to the median 5-m R_ρ in layers where intrusive features are infrequent. The near-surface layer contains the largest variability of 5-m R_ρ, with intrusive features also occurring at $\overline{z} > 600$ m. These later features are associated with the upper boundary of the Mediterranean-property tongue. Figure 13b shows estimates of the diffusivities derived from (14). The haline diffusivity is enhanced over the thermal diffusivity in the upper thermocline, 150 m $< \overline{z} < 450$ m, where 0.5-m scale patches are characterized by $R_\rho < 2$. Near $\overline{z} = 500$ m, the two diffusivities converge as $R_\rho \gtrsim 2$. However, beneath $\overline{z} = 650$ m, low-R_ρ patches attributable to intrusive features are adequate to enhance k_s over k_θ even though the large-scale stratification is characterized by $\overline{R_\rho} \approx 2.5$. Also shown are the estimates of the tracer diffusivity reported by Ledwell et al. (1998). The tracer was released at the $\sigma_\theta = 26.75$ kg m^{-3} isopycnal, close to the $\overline{z} = 300$ m neutral surface used in our analysis. The eddy diffusivity of the chemical tracer (sulfur hexafluoride) is expected to be equal to that of salt. Our estimate of k_s agrees best with the tracer estimate derived for May 1992 through November 1992, the period immediately following the HRP survey. Figure 13c shows the diffusivity of density (k_ρ) inferred from k_θ and k_s using the relation

$$k_\rho \overline{N^2} = g \left[\alpha(k_\theta \overline{\Theta}_z) - \beta(k_s \overline{S}_z) \right]. \qquad (15)$$
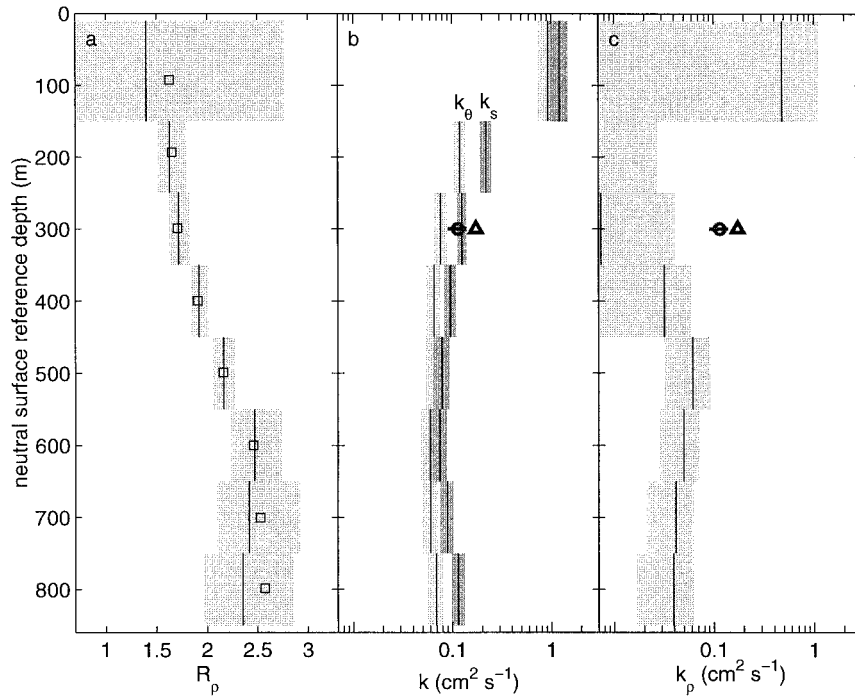
FIG. 13. Results from the analysis of neutral density layers at the NATRE site. The mean depth of the neutral surfaces are used as the reference vertical coordinate. (a) The density ratio structure of each layer is shown. The shaded box is the interquartile range of the 5-m R_ρ, with the median value shown as the vertical line. The large-scale density ratio is computed from the layer-averaged $\overline{\Theta_z}$, and $\overline{S_z}$, and this value is shown in each box by the open square. (b) Profiles of the thermal (k_θ) and haline (k_s) vertical diffusivities. The tracer-derived diffusivities (Ledwell et al. 1998) at the $\overline{z} = 300$ m surface are also shown. The circle gives the tracer-derived estimate for May–November 1992, the period closest in time to the HRP survey. The triangle gives the average tracer diffusivity over the latter 2 years of the experiment (November 1992–November 1994). If the vertical diffusivities of heat and salt differ, the tracer diffusivity should be that of salt. (c) The diffusivity of density derived from k_θ and k_s using $k_\rho \overline{N^2} = g(\alpha k_\theta \overline{\Theta_z} - \beta k_s \overline{S_z})$. The relative sizes of error bars in (b) and (c) is skewed by the logarithmic x-axis.

In the upper 300 m, k_ρ is near zero and possibly negative. The diffusivity for density is less than k_θ and k_s in all layers where $k_s > k_\theta$. Furthermore, k_ρ clearly underestimates the tracer derived diffusivity. At $\overline{z} = 500$ m, where fingers contribute little dissipation, the diffusivities are nearly equal.

b. Estimates of diapycnal advection

With estimates of the vertical diffusivities derived from (14), we may estimate not only the vertical fluxes of heat and salt, but also the vertical flux divergence of buoyancy. The flux divergence of buoyancy is of interest because it will dictate the strength of the advection between layers of different density. This diapycnal advection (w_*) is strictly the diapycnal component of the total vertical velocity, $w_{(total)} = \mathbf{u} \cdot \nabla z_n + w_*$, where z_n is the interface between two neutral density layers (Pedlosky 1996). An equation for the diapycnal advection has been derived by McDougall (1991). Here we use a form of the McDougall (1991) expression suitable for

vertical differentiation in a layered neutral density system with nonequal thermal and haline diffusivities,

$$w_* = g(\overline{N^2})^{-1}[\alpha \sigma_z \partial_\sigma (k_\theta \overline{\Theta_z}) - \beta \sigma_z \partial_\sigma (k_s \overline{S_z})]$$
$$- g(\overline{N^2})^{-1} \kappa [C_b \nabla \overline{\Theta} \cdot \nabla \overline{\Theta} + T_b \nabla \overline{\Theta} \cdot \nabla \overline{P}]. \quad (16)$$

where σ and σ_z are neutral density and its vertical derivative. In (16), κ is the epineutral diffusivity (i.e., the diffusivity acting along neutral surfaces), ∇ is the epineutral gradient operator, and $\overline{P}$ is the pressure along the neutral surface. Thus, the diapycnal velocity depends not only on the vertical-flux divergence of density, but also on the lateral divergence of $\overline{\Theta}$ and $\overline{S}$ fluxes by mesoscale eddies. Since neutral surfaces are defined by the relation $\alpha \nabla \overline{\Theta} = \beta \nabla \overline{S}$, epineutral fluxes are divergent only through the nonlinear terms in the equation of state. In particular, the process of cabbeling is represented through the term $C_b \nabla \overline{\Theta} \cdot \nabla \overline{\Theta}$, with $C_b \sim \partial \alpha / \partial \Theta$. The second nonlinear thermodynamic process is the so-called thermobaric effect, represented by $T_b \nabla \overline{\theta} \cdot \nabla \overline{P}$ with $T_b \sim \partial \alpha / \partial p$. We further note that (16) is the complete specification of the advection through

TABLE 2. Components of the dianeutral advection.

z (m)	$g(\overline{N^2})^{-1}\alpha\sigma_z\partial(k_\theta\overline{\Theta_z})/\partial\sigma$ (m yr^{-1})	$-g(\overline{N^2})^{-1}\beta\sigma_z\partial(k_s\overline{S_z})/\partial\sigma$ (m yr^{-1})	$-g(\overline{N^2})^{-1}\kappa C_b\nabla\overline{\Theta}\cdot\nabla\overline{\Theta}$ (m yr^{-1})	$-g(\overline{N^2})^{-1}\kappa T_b\nabla\overline{\Theta}\cdot\nabla\overline{P}$ (m yr^{-1})	w_* (m yr^{-1})
90			-0.48 ± 0.24	-0.02 ± 0.01	
190	23.24 ± 5.19	-20.18 ± 4.65	-0.10 ± 0.05	0.00 ± 0.00	2.96 ± 6.96
300	3.64 ± 0.86	-5.33 ± 0.89	-0.03 ± 0.01	0.01 ± 0.00	-1.71 ± 1.24
400	1.24 ± 0.60	-2.26 ± 0.38	-0.02 ± 0.01	0.01 ± 0.00	-1.03 ± 0.71
500	0.80 ± 0.50	-1.15 ± 0.28	-0.02 ± 0.01	0.01 ± 0.00	-0.36 ± 0.58
600	0.43 ± 0.51	-0.24 ± 0.24	-0.01 ± 0.01	0.00 ± 0.00	0.18 ± 0.57
700	-0.18 ± 0.43	0.24 ± 0.21	-0.14 ± 0.07	-0.01 ± 0.01	-0.09 ± 0.49
800			-0.54 ± 0.27	0.00 ± 0.01	

a neutral surface. The equation is appropriate for fully three-dimensional flow.

The vertical-flux divergence contribution to w_* was computed by differentiating the vertical fluxes of heat ($F_\theta = -k_\theta\overline{\Theta}_z$) and salt ($F_s = -k_s\overline{S}_z$) using a central-difference scheme with an associated error propagation formula. The epineutral contributions to the diapycnal advection were also estimated. An epineutral diffusivity of $\kappa = 1000 \pm 500$ m^2 s^{-1} was used in these calculations. This κ is consistent with the value reported by Ledwell et al. (1998) for the lateral diffusivity acting along the tracer release surface. The epineutral gradients of $\overline{\Theta}$ and $\overline{P}$ were calculated from the hydrography of the NATRE HRP survey. The $\overline{\Theta}$ and $\overline{P}$ fields were mapped onto a quadratic plane of the form

$$\Phi(X, Y) = \phi_0 + \phi_x X + \phi_y Y + \phi_{xx} X^2 + \phi_{xy} XY + \phi_{yy} Y^2, \tag{17}$$

where (X, Y) are the Cartesian coordinates centered on the survey, and $\phi(\cdot)$ are the coefficients of the least square fit. Degrees of freedom in the lateral scalar fields were determined by examining spatial-lag correlations. While all 100 stations are treated as independent for the $\overline{\Theta}$ calculations, the $\overline{P}$ field contained only 50 independent samples. The standard errors of the scalar fields were used with the least square fits to provide uncertainty of the lateral gradient quantities. We evaluated (17) at the interpolated point centered within the HRP survey grid. These central estimates are then used with the net diffusivities given by (16).
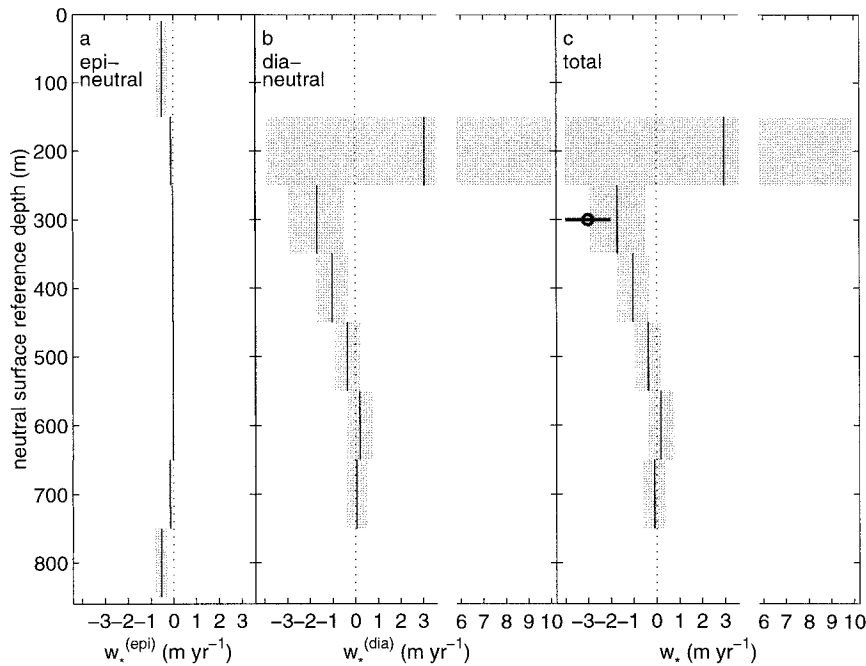

FIG. 14. The diapycnal advection w_* computed using the profiles of k_θ and k_s shown in Fig. 13b. (a) The epineutral component of the diapycnal advection. This small contribution comes mainly from the cabbeling term. (b) The diapycnal-flux component of the diapycnal advection. Only layers at $\overline{z} = 300$ m and $\overline{z} = 400$ m have contributions distinguishable from zero. (c) The total diapycnal advection $w_* = w_*^{(epi)} + w_*^{(dia)}$. The downward advection at the $\overline{z} = 300$ m surface is consistent with the tracer-derived result (Ledwell et al. 1998) shown as the circle with error bar.
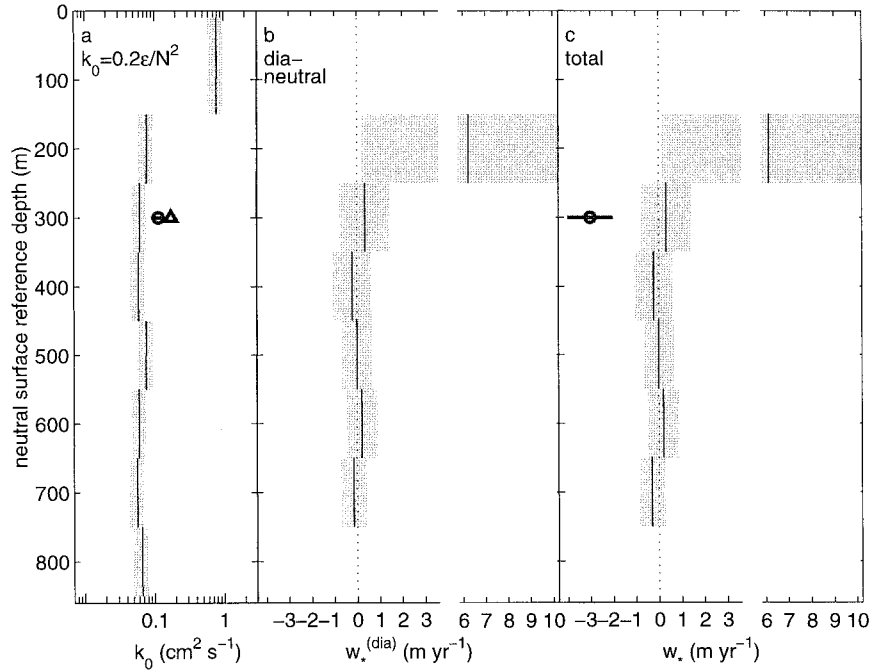
FIG. 15. The diapycnal advection w_* when no salt-finger enhancement of the haline diffusivity is used. (a) The scalar diffusivity of turbulence $k_0 = 0.2\langle\epsilon\rangle(\overline{N^2})^{-1}$ (Osborn 1980). The tracer-derived diffusivities for May–November 1992 (circle) and November 1992 through November 1994 (triangle) are shown at the $\overline{z} = 300$ m surface. (b) The diapycnal contribution to the advection. (c) The total diapycnal advection (with the epineutral component from Fig. 14a). With no salt-finger enhancement of k_s, the advection at the tracer-release depth is no longer distinguishable from zero.

Estimates of the diapycnal advection are given in Table 2 and plotted in Fig. 14. The epineutral contribution to w_* [i.e., $w_*^{(epi)} = -g(\overline{N^2})^{-1}\kappa[C_b\nabla\overline{\Theta} \cdot \nabla\overline{\Theta}] - g(\overline{N^2})^{-1}\kappa[T_b\nabla\overline{\Theta} \cdot \nabla\overline{P}]$] turns out to be small, as is shown in Fig. 14a. The cabbeling term is nonzero in the few layers with nonzero $w_*^{(epi)}$. The thermobaric term is generally very small. The diapycnal flux contribution to w_* [i.e., $w_*^{(dia)} = g(\overline{N^2})^{-1}[\alpha\sigma_z\partial_\sigma(k_\theta\overline{\Theta}_z) - \beta\sigma_z\partial_\sigma(k_s\overline{S}_z)]$], using the net diffusivities given by Table 1, is shown in Fig. 14b. We do not report estimates for the upper and lower layers due to the use of a central difference in computing the divergence of the vertical fluxes. The uppermost layer with reported $w_*^{(dia)}$ corresponds to 150 m $< \overline{z} < 250$ m. The diapycnal velocity in this layer is known very poorly, owing to the large uncertainty of the surface-layer fluxes. Figure 14c shows the sum of $w_*^{(epi)}$ and $w_*^{(dia)}$, giving the total diapycnal advection w_*. Two layers ($\overline{z} = 300$ m and $\overline{z} = 400$ m) are characterized by negative (downward) advection. In particular, the $\overline{z} = 300$ m surface shows downward advection of $w_* = -(1.7 \pm 1.2)$ m yr^{-1} ($w_* \approx 6 \times 10^{-8}$ m s^{-1}). A value for the diapycnal velocity in this layer was also reported by Ledwell et al. (1998), based on sinking of the tracer distribution relative to the release isopycnal. The Ledwell et al. (1998) estimate of $w_* = -(3 \pm 1)$ m yr^{-1} is shown in the figure and is within one standard error of our estimate.

We now contrast diapycnal advection estimates presented above with estimates based on an alternate approach. The Osborn (1980) model was used to calculate a net diffusivity k_0, based on the assumption that dissipation is solely due to turbulence. With no salt-finger enhancement of k_s, all scalars have the same vertical diffusivity, $k_\theta = k_s = k_0$, and the diapycnal-flux divergence components of the diapycnal advection can be expressed as

$$w_*^{(dia)} = g(\overline{N^2})^{-1}\left[g^{-1}\sigma_z\frac{\partial}{\partial\sigma}(k_0\overline{N^2}) - k_0\frac{\partial\alpha}{\partial\theta}\overline{\Theta}_z^2\right]$$

$$= g(\overline{N^2})^{-1}\left[g^{-1}\Gamma^{(t)}\sigma_z\frac{\partial\epsilon}{\partial\sigma} - \frac{\partial\alpha}{\partial\theta}\frac{\langle\chi\rangle}{2}\right], \qquad (18)$$

where the relations $k_0\overline{N^2} = \Gamma^{(t)}\langle\epsilon\rangle$ and $k_0\overline{\Theta}_z^2 = 0.5\langle\chi\rangle$ have been used. Figure 15 shows the alternate estimates of diapycnal advection. The net diffusivity estimated by $k_0 = 0.2\langle\epsilon\rangle(\overline{N^2})^{-1}$ is shown in Fig. 15a. This diffusivity is slightly less than the previously estimated k_θ and k_s. Figure 15b shows the diapycnal component of the advection, given by (18). The diapycnal component of the advection was added to the previously estimated epineutral component and the total diapycnal velocity is shown in Fig. 15c. This approach dictates that all layers beneath the influence of the mixed layer have diapycnal

advection indistinguishable from zero. The best agreement between the microstructure- and tracer-derived mixing rates is achieved when the salt-finger enhancement of k_s is accounted for.

5. Discussion

We have shown that elevated dissipation events are related to stability parameters characterizing the locale where the mixing is occurring. Elevated χ ($\chi > 1 \times 10^{-9}$ K^2 s^{-1}) can be associated with either turbulence or salt fingers based on the local values of the density ratio or Richardson number. Dissipation rates χ and ϵ were examined with respect to the two processes through the use of the nondimensional dissipation ratio Γ. Approximately 70% of the elevated χ data was consistent with the dissipation ratio of turbulence. These observations were generally associated with Ri < 1 (65% of the elevated χ). Data with ($R_\rho > 2$, Ri > 1) were also characterized by Γ consistent with the turbulence model. The remaining elevated χ occurred when ($R_\rho < 2$, Ri > 1). The dissipation ratio of these observations was inconsistent with the turbulence model. Instead, Γ of the ($R_\rho < 2$, Ri > 1) data was found to be consistent with the model for fingers. Thus, when the Richardson number exceeds unity, there is a general transition at $R_\rho \sim 2$ between a turbulent-dominated and finger-dominated regime. Only 3% of elevated χ observations fall outside the generalizations referred to above. Observations binned in the parameter range ($1.1 < R_\rho < 1.3$, $0.3 < $ Ri < 1) are consistent with salt fingers, while the ($2 < R_\rho < 4$, $10 < $ Ri < 30) observations were inconsistent with either model.

The dissipation ratio analysis clearly rejects the notion that salt fingers are important throughout the general range of finger-favorable stratification ($1 < R_\rho < 100$). On the contrary, most elevated χ data meet the dissipation ratio criterion for turbulence. However, evidence for fingers is strong when the stability parameters fall in the range ($1 < R_\rho < 2$, Ri > 1). Our finding, that fingers are constrained to this narrow range of density ratio and Richardson number, supports conclusions of previous studies. Schmitt and Evans (1978) argued that growing modes of the finger instability overcome wave-strained gradients of Θ and S only when $R_\rho < 2$. Schmitt (1981) pointed out that the occurrence of thermohaline staircases is confined to $R_\rho < 1.7$. Additionally, Linden (1974) used theory and experiment to show that weak shear permits fingers in the form of sheets aligned with the flow. Kunze (1994) has considered time-dependent shear and found that finger sheets will be tilted as the shear vector turns with time. However, at $R_\rho < 2$, vertical finger fluxes remain strong.

The formal examination of the parameter space (R_ρ, Ri, Γ) presented here included only elevated dissipation rate observations of the form $\chi > 1 \times 10^{-9}$ K^2 s^{-1}. For elevated levels of χ, there is a partition finger and turbulence regimes. However, since the distributions of ϵ and χ are roughly lognormal, the exceptional events dominate the ensemble average. These ensemble averages dictate the magnitude of the vertical diffusivities. Thus, we expect the conclusions drawn about the association of salt fingers and turbulence with the stability parameters to apply not only to exceptional dissipation, but more generally to average dissipation.

We have implemented a method for estimating the diapycnal fluxes driven by both turbulent and salt-finger mixing events. The calculations involve partitioning observations of ϵ and χ into finger-favorable and turbulent conditions using the local values of R_ρ and Ri. For each class of dissipation, we calculate the thermal diffusivity using the production–dissipation balances (1) and (2). The haline diffusivity is set equal to k_θ for the ensemble of data not favorable to fingers. However, k_s for the finger-favorable ensemble is calculated by enhancing the thermal diffusivity by the factor R_ρ/r, with $r = (\alpha k_\theta \overline{\Theta_z})(\beta k_s \overline{S_z})^{-1}$ known from laboratory measurements of salt fingers to be $r = 0.6 \pm 0.04$ when $R_\rho < 2$. A model for enhancing the haline flux in a region experiencing both turbulence and fingers was proposed by McDougall and Ruddick (1992, hereafter MR92). As we have done in (14), the MR92 model expresses vertical fluxes in terms of a sum between the turbulent and salt-finger derived dissipation. The MR92 model relies on algebraic relations between Γ, $\Gamma^{(t)}$, and $\Gamma^{(f)}$ to give the relative weights between the turbulent and finger-derived fluxes; we found this approach overly sensitive to uncertainty in the dissipation rate estimates. In contrast, in our approach the weighting factors $P^{(t)}$ and $P^{(f)}$ are determined directly from observations of R_ρ and Ri. Our analysis of the dissipation ratio was not critically dependent on the values for $\Gamma^{(t)}$ and $\Gamma^{(f)}$. Instead, our analysis served to show that a reasonable relationship exists between R_ρ, Ri and the dissipation ratio. We believe that our method for calculating diffusivities is the more relevant application of the information available in profiles of fine- and microstructure variables.

Our estimates of vertical diffusivities imply that salt fingers act to enhance k_s over k_θ by about 60% at depths near the NATRE tracer-release surface. These diffusivities were used to calculate the diapycnal fluxes of heat and salt, and the divergences of these fluxes dictate the diapycnal advection. In both layers found to have downward advection ($\overline{z} = 300$ m and $\overline{z} = 400$ m), the divergence of the haline-flux dominates over the thermal-flux divergence. To better understand the physical processes that determine w_*, we have dissected the diapycnal-flux divergence terms in the diapycnal advection equation into the form

$$w_*^{(\text{dia})} = g(\overline{N^2})^{-1}\left(\alpha \sigma_z \frac{\partial k_\theta}{\partial \sigma}\overline{\Theta_z} + \alpha \sigma_z k_\theta \frac{\partial \overline{\Theta_z}}{\partial \sigma} - \beta \sigma_z \frac{\partial k_s}{\partial \sigma}\overline{S_z} \right.$$
$$\left. - \beta \sigma_z k_s \frac{\partial \overline{S_z}}{\partial \sigma}\right). \qquad (19)$$

TABLE 3. Flux components of the dianeutral advection equation.

z (m)	$g(\overline{N^2})^{-1}\alpha\sigma_z\dfrac{\partial k_\theta}{\partial\sigma}\overline{\Theta}_z$ (m yr⁻¹)	$+g(\overline{N^2})^{-1}\alpha\sigma_z k_\theta\dfrac{\partial\overline{\Theta}_z}{\partial\sigma}$ (m yr⁻¹)	$-g(\overline{N^2})^{-1}\beta\sigma_z\dfrac{\partial k_s}{\partial\sigma}\overline{S}_z$ (m yr⁻¹)	$-g(\overline{N^2})^{-1}\beta\sigma_z k_s\dfrac{\partial\overline{S}_z}{\partial\sigma}$ (m yr⁻¹)	$w_*^{(epi)}$ (m yr⁻¹)	w_* (m yr⁻¹)
90					−0.51	
190	14.70	−0.25	−11.32	−0.07	−0.10	2.96
300	2.39	1.62	−3.20	−2.49	−0.02	−1.71
400	0.25	0.93	−0.84	−1.35	−0.01	−1.03
500	0.28	1.22	−0.50	−1.36	−0.01	−0.36
600	0.25	0.17	0.11	−0.33	−0.01	0.18
700	−0.20	0.04	0.35	−0.13	−0.15	−0.09
800					−0.54	

Thus, the divergence of the diapycnal fluxes are written as two terms: a term proportional to the derivative of the diffusivity and a term proportional to the derivative of the respective heat or salt gradient. The values of these terms are given in Table 3. Advection through the $\overline{z} = 300$ m surface is most influenced by the vertical change of k_s, while the $\overline{z} = 400$ m surface is more determined by the vertical change of $\overline{S}_z$. In these layers, salt extracted from above increases the density of the resident parcels causing them to sink. This occurs despite the fact that resident parcels are also being heated. In this manner, salt-finger density fluxes act to oppose the traditional view of upwelling in the thermocline (Robinson and Stommel 1959).

Several models have been proposed that parameterize salt-finger fluxes in terms of the density ratio. The Schmitt (1981) model is ad hoc, with a power-law dependence that allows a considerable enhancement of k_s at low density ratios. One aspect of the Schmitt (1981) model is the tendency for finger fluxes to maintain a tight Θ–S relation. Supporting evidence for this is found in the comparison of 5-m R_ρ with the $O(100$ m$)$ R_ρ in Fig. 13. These data suggest that the Θ–S relation is
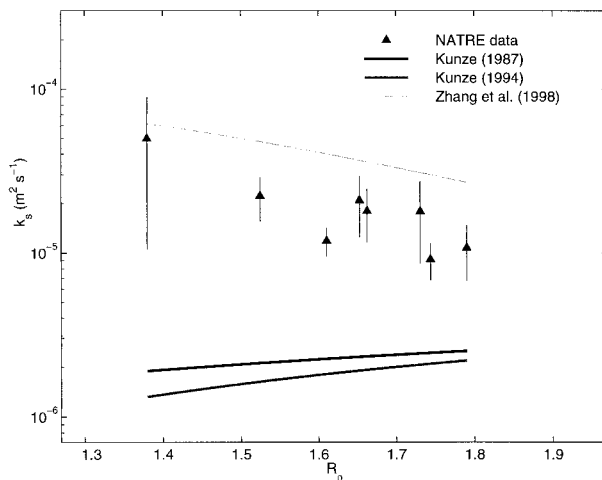

FIG. 16. Comparison of the finger diffusivities for salt as estimated by the NATRE microstructure and salt-finger models. The Kunze (1987, 1994) models are based on stability considerations. The Zhang et al. (1998) model is based on the the Schmitt (1981) ad hoc model.

tightest in the depth range 200 m $< \overline{z} <$ 600 m where the fingers are most active. Zhang et al. (1998) have refined the Schmitt (1981) model such that the haline diffusivity is given by $k_s = (1 \times 10^{-4}$ m² s⁻¹$)[1 + (R_\rho/1.6)^6]^{-1}$. Another set of models that predict finger-fluxes subject to a dynamical constraint have been proposed by Kunze (1987, 1994). These models use a finger Richardson number constraint that is similar to the Stern (1969) Reynolds number constraint. The dissipation data from NATRE provides an opportunity to examine the applicability to these models to thermocline mixing. We have calculated finger-driven haline diffusivities using (12) and (13) with the 5-m scale Θ–S gradients. These diffusivities are compared with diffusivites predicted by Zhang et al. (1998) and Kunze (1987, 1994) in Fig. 16. The Kunze (1987, 1994) models predict an increase in diffusivity with R_ρ not exhibited by the NATRE data. The relation used by Zhang et al. (1998) is a bit more diffusive than the data suggest, as may be appropriate for the larger-scale gradients used by the model, but has a density ratio dependence that is qualitatively correct.

In terms of the vorticity budget for the upper thermocline, the diapycnal advection we have documented would play a limited role. Specifically, "stretching" of fluid columns in the upper ocean given by $f\partial_z w_{(\text{total})}$ would be dominated by the adiabatic component of vertical velocity $\mathbf{u} \cdot \nabla z_n$, which is set by the Ekman pumping through the mixed layer. Joyce et al. (1998) estimate the Ekman downwelling applicable to the NATRE region to be ~40 m yr⁻¹. Thus, the diabatic forcing we have discussed makes up ≤10% of the total vertical velocity in the ventilated thermocline.

However, at depths not influenced by Ekman pumping, diabatic forcing will dominate the total vertical velocity and the vortex stretching. In particular, the underside of the Mediterranean property core is strongly favorable to salt fingers. Salt-finger fluxes in this region would drive downward advection beneath the core. Spall (1999) has examined the circulation in this region and found that vortex stretching by salt-finger driven advection would produce a circulation consistent with observations. Furthermore, the diapycnal fluxes we have documented must be of consequence

to the long timescale density budget. Models of the thermohaline circulation suggest that the efficiency of the oceanic heat transport is strongly influenced by differences between the vertical diffusivities k_θ and k_s (Gargett and Ferron 1996; Zhang et al. 1998). In particular, these models find that salt fingering in the upper thermocline decreases the strength of the meridional overturning cell. This is because salt fingers drive an upgradient density flux, and upgradient density flux is detrimental to the vertical advective–diffusive balance that closes the thermohaline cell. As demonstrated by the NATRE data, the microstructure observations allow for estimation of the salt-finger component of the mixing. These salt-finger estimates are crucial in explaining the downward diapycnal–advection of tracer, as turbulent mixing alone cannot account for an upgradient density flux. Thus, we suggest that expanded use of the techniques developed here will be important in determining the influence of salt fingering on the general circulation.

REFERENCES

Baker, M. A., and C. H. Gibson, 1987: Sampling turbulence in the stratified ocean: Statistical consequences of strong intermittency. *J. Phys. Oceanogr.,* **17,** 1817–1836.

Bevington, P. R., and D. K. Robinson, 1992: *Data Reduction and Error Analysis for the Physical Sciences.* McGraw-Hill, 328 pp.

Davis, R. E., 1996: Sampling turbulent dissipation. *J. Phys. Oceanogr.,* **26,** 341–358.

Efron, B., and G. Gong, 1983: A leisurely look at the bootstrap, the jackknife, and cross-validation. *Amer. Stat.,* **37,** 36–48.

Gargett, A. E., and B. Ferron, 1996: The effects of differential vertical diffusion of T and S in a box model of thermohaline circulation. *J. Mar. Res.,* **54,** 827–866.

Haldane, J. B. S., 1952: Simple tests for bimodality and bitangentiality. *Ann. Eugen.,* **16,** 359–364.

Hamilton, J. M., M. R. Lewis, and B. R. Ruddick, 1989: Vertical fluxes of nitrate associated with salt fingers in the world's oceans. *J. Geophys. Res.,* **94,** 2137–2145.

Huq, P., and R. E. Britter, 1995: Turbulence evolution and mixing in a two layer stably stratified fluid. *J. Fluid Mech.,* **285,** 41–67.

Jackett, D. R., and T. J. McDougall, 1997: A neutral density variable for the world's oceans. *J. Phys. Oceanogr.,* **27,** 237–263.

Joyce, M. T., J. R. Luyten, A. Kubryakov, F. B. Bahr, and J. S. Pallant, 1998: Meso- to large-scale structure of subducting water in the subtropical gyre of the eastern North Atlantic Ocean. *J. Phys. Oceanogr.,* **28,** 40–61.

Kunze, E., 1987: Limits on growing, finite-length salt fingers: A Richardson number constraint. *J. Mar. Res.,* **45,** 533–556.

——, 1990: The evolution of salt fingers in inertial wave shear. *J. Mar. Res.,* **48,** 471–504.

——, 1994: A proposed flux constraint for salt fingers in shear. *J. Mar. Res.,* **52,** 999–1016.

——, and J. M. Toole, 1997: Tidally driven vorticity, diurnal shear, and turbulence atop Fieberling Seamount. *J. Phys. Oceanogr.,* **27,** 2663–2693.

——, A. J. Williams, and R. W. Schmitt, 1987: Optical microstructure in the thermohaline staircase east of Barbados. *Deep-Sea Res.,* **34,** 1697–1704.

Ledwell, J. R., A. J. Watson, and C. S. Law, 1993: Evidence for slow mixing across the pycnocline from an open-ocean tracer-release experiment. *Nature,* **364,** 701–703.

——, ——, and ——, 1998: Mixing of a tracer released in the pycnocline of a subtropical gyre. *J. Geophys. Res.,* **103,** 21 499–21 529.

Linden, P. F., 1974: Salt fingers in a steady shear flow. *Geophys. Fluid Dyn.,* **6,** 1–27.

Lueck, R., 1987: Microstructure measurements in a thermohaline staircase. *Deep-Sea Res.,* **34,** 1677–1688.

McDougall, T. J., 1991: Water mass analysis with three conservative variables. *J. Geophys. Res.,* **96,** 8687–8693.

——, and J. R. Taylor, 1984: Flux measurements across a finger interface at low values of the stability ratio. *J. Mar. Res.,* **42,** 1–14.

——, and B. R. Ruddick, 1992: The use of ocean microstructure to quantify both turbulent mixing and salt fingering. *Deep-Sea Res.,* **39,** 1931–1952.

Moum, J. N., 1996: Efficiency of mixing in the main thermocline. *J. Geophys. Res.,* **101,** 12 057–12 069.

Oakey, N. S., 1985: Statistics of mixing parameters in the upper ocean during JASIN phase 2. *J. Phys. Oceanogr.,* **15,** 1662–1675.

Osborn, T. R., 1980: Estimates of the local rate of vertical diffusion from dissipation measurements. *J. Phys. Oceanogr.,* **10,** 83–89.

——, and C. S. Cox, 1972: Oceanic fine structure. *Geophys. Fluid Dyn.,* **3,** 321–345.

Pedlosky, J., 1996: *Ocean Circulation Theory.* Springer-Verlag, 453 pp.

Polzin, K. L., 1996: Statistics of the Richardson number: Mixing models and finestructure. *J. Phys. Oceanogr.,* **26,** 1409–1425.

——, and E. T. Montgomery, 1996: Microstructure profiling with the High Resolution Profiler. *Proc. ONR Workshop on Microstructure Sensors,* Mt. Hood, OR, 109–115.

Robinson, A. R., and H. Stommel, 1959: The oceanic thermocline and the associated thermohaline circulation. *Tellus,* **11,** 295–308.

Rohr, J. J., E. C. Itsweire, and C. W. Van Atta, 1984: Mixing efficiency in stably-stratified decaying turbulence. *Geophys. Astrophys. Fluid Dyn.,* **29,** 221–236.

Ruddick, B., D. Walsh, and N. Oakey, 1997: Variations in apparent mixing efficiency in the North Atlantic Central Water. *J. Phys. Oceanogr.,* **27,** 2589–2605.

Schmitt, R. W., 1979a: The growth rate of super-critical salt fingers. *Deep-Sea Res.,* **26,** 23–40.

——, 1979b: Flux measurements on salt fingers at an interface. *J. Mar. Res.,* **37,** 419–436.

——, 1981: Form of the temperature-salinity relationship in the Central Water: Evidence for double-diffusive mixing. *J. Phys. Oceanogr.,* **11,** 1015–1026.

——, 1990: On the density ratio balance in Central Water. *J. Phys. Oceanogr.,* **20,** 900–906.

——, 1994: Double diffusion in oceanography. *Annu. Rev. Fluid Mech.,* **26,** 255–285.

——, and D. L. Evans, 1978: An estimate of the vertical mixing due to salt fingers based on observations of North Atlantic Central Water. *J. Geophys. Res.,* **83,** 2913–2919.

——, H. Perkins, J. D. Boyd, and M. C. Stalcup, 1987: C-SALT: An investigation of the thermohaline staircase in the western tropical North Atlantic. *Deep-Sea Res.,* **34,** 1655–1665.

——, J. M. Toole, R. L. Koehler, E. C. Mellinger, and K. W. Doherty, 1988: The development of a fine- and microstructure profiler. *J. Atmos. Oceanic Technol.,* **5,** 484–500.

Shen, C. Y., 1993: Heat-salt finger fluxes across a density interface. *Phys. Fluids A,* **5,** 2633–2643.

——, 1995: Equilibrium salt-fingering convection. *Phys. Fluids A,* **7,** 706–717.

Spall, M. A., 1999: A simple model of the large scale circulation of Mediterranean Water and Labrador Sea Water. *Deep-Sea Res.,* **46,** 181–204.

Stern, M. E., 1969: Collective instability of salt fingers. *J. Fluid Mech.,* **35,** 209–218.

——, 1975: *Ocean Circulation Physics.* Academic Press, 246 pp.

——, and J. S. Turner, 1969: Salt fingers and convecting layers. *Deep-Sea Res.,* **16,** 497–511.

Taylor, J., and P. Bucens, 1989: Laboratory experiments on the structure of salt fingers. *Deep-Sea Res.,* **36,** 1675–1704.

Toole, J. M., K. L. Polzin, and R. W. Schmitt, 1994: Estimates of diapycnal mixing in the abyssal ocean. *Science,* **264,** 1120–1123.

——, R. W. Schmitt, K. L. Polzin, and E. Kunze, 1997: Near-boundary mixing above the flanks of a midlatitude seamount. *J. Geophys. Res.,* **102,** 947–959.

Turner, J. S., 1967: Salt fingers across a density interface. *Deep-Sea Res.,* **14,** 599–611.

Yamazaki, H., and T. R. Osborn, 1990: Dissipation estimates for stratified turbulence. *J. Geophys. Res.,* **95,** 9739–9744.

Zhang, J., R. W. Schmitt, and R. X. Huang, 1998: Sensitivity of the GFDL Modular Ocean Model to the parameterization of double-diffusive processes. *J. Phys. Oceanogr.,* **28,** 589–605.